Two/Quasi-two-dimensional perovskite-based heterostructures: construction, properties and applications

OPEN ACCESS
IOP Publishing | IMMT
International Journal of Extreme Manufacturing
Int. J. Extrem. Manuf. **5** (2023) 012004 (24pp)
https://doi.org/10.1088/2631-7990/acab40

Topical Review

Two/Quasi-two-dimensional perovskite-based heterostructures: construction, properties and applications

Haizhen Wang[1,3], **Yingying Chen**[1,3] and **Dehui Li**[1,2,*]

[1] School of Optical and Electronic Information, Huazhong University of Science and Technology, Wuhan 430074, People's Republic of China
[2] Wuhan National Laboratory for Optoelectronics, Huazhong University of Science and Technology, Wuhan 430074, People's Republic of China

E-mail: dehuili@hust.edu.cn

Received 19 October 2022, revised 18 November 2022
Accepted for publication 13 December 2022
Published 23 January 2023

Abstract

Two-dimensional (2D)/quasi-2D organic-inorganic halide perovskites are regarded as naturally formed multiple quantum wells with inorganic layers isolated by long organic chains, which exhibit layered structure, large exciton binding energy, strong nonlinear optical effect, tunable bandgap via changing the layer number or chemical composition, improved environmental stability, and excellent optoelectronic properties. The extensive choice of long organic chains endows 2D/quasi-2D perovskites with tunable electron-phonon coupling strength, chirality, or ferroelectricity properties. In particular, the layered nature of 2D/quasi-2D perovskites allows us to exfoliate them to thin plates to integrate with other materials to form heterostructures, the fundamental structural units for optoelectronic devices, which would greatly extend the functionalities in view of the diversity of 2D/quasi-2D perovskites. In this paper, the recent achievements of 2D/quasi-2D perovskite-based heterostructures are reviewed. First, the structure and physical properties of 2D/quasi-2D perovskites are introduced. We then discuss the construction and characterizations of 2D/quasi-2D perovskite-based heterostructures and highlight the prominent optical properties of the constructed heterostructures. Further, the potential applications of 2D/quasi-2D perovskite-based heterostructures in photovoltaic devices, light emitting devices, photodetectors/phototransistors, and valleytronic devices are

[3] Contributed equally to this work.
[*] Author to whom any correspondence should be addressed.

2631-7990/23/012004+24$33.00

demonstrated. Finally, we summarize the current challenges and propose further research directions in the field of 2D/quasi-2D perovskite-based heterostructures.

Keywords: 2D perovskites, heterostructures, characterization, optical properties, applications

1. Introduction

Heterostructures [1], integrating two or more dissimilar materials together, are not only fundamental building blocks for functional optoelectronic devices [2–9] such as photovoltaic solar cells [10–12], light emitting diodes (LEDs) [13, 14], and photodetectors [15, 16], they are also essential platforms for the investigation of optical or optoelectronic properties of semiconductors. Some unique physical properties, which are not present within individual constituent components, can be observed through the interface modulation among heterostructures. Besides, energy band alignment among semiconductor interfaces induced by interface modulation leads to unprecedented physical phenomena/properties of semiconductors [17], e.g. energy/charge transfer [18–21] and interlayer excitons [22, 23], which thus result in extended functionalities for optoelectronic heterostructure devices.

Conventional heterostructures are generally composed of materials with covalent bonds, which require each constituent component to have well-matched lattices. Originally, heterostructures were mostly constructed with III–IV or II–VI group semiconductors [24]. Until recently, with the advancement of new techniques to obtain materials with atomic level thickness, two-dimensional (2D) layered materials [25], including graphene [26, 27], transitional metal dichalcogenides (TMDs) [28], black phosphorous (BP) [29], and carbon-based materials [30] have been promising candidates for constructing heterostructures with novel functionalities, which have shown potential applications in optoelectronic devices due to their unique layered property. These atomically thin materials exhibit special physical and optoelectronic properties, which can be further modulated by doping [31, 32] or exerting external fields, such as strain [33–36], electrical [37–41], or magnetic field [42–44]. Since those layered materials are bounded together via weak Van der Waals forces, they can be easily exfoliated into thin flakes without dangle bonds at their surface. Therefore, lattice match in heterostructures consisting of those layered material flakes is not required and the interface quality can be greatly improved, which enables us to stack them layer by layer to build unique heterostructures with unprecedented physical properties in view of the wide range of 2D materials we can select.

As a new member of the 2D material family, two-dimensional and quasi-two-dimensional perovskites (both abbreviated to 2D perovskites hereafter) have attracted increasing attention due to their excellent properties, such as large exciton binding energy, high photoluminescence (PL) quantum efficiency, large oscillator strengths, and long carrier diffusion length, and thus are emerging candidates for next-generation optoelectronic devices [45–51]. 2D perovskites not only inherit the properties of 2D materials, but also possess the excellent optoelectronic properties of organic-inorganic halide perovskites, which were extensively studied in the last decade due to their extremely rapid soared power conversion efficiency (PCE) [52]. 2D perovskites can be considered as a repetition of an inorganic layer sandwiched between two organic spacer layers, which are natural quantum wells with large exciton binding energy [53, 54]. The dielectric constant difference between organic ligand barrier and inorganic octahedral layers causes the dielectric confinement effect, resulting in huge oscillator strengths and large exciton binding energy [55–57]. The intrinsic superior environmental stability of 2D perovskites, in contrast to their three-dimensional (3D) counterparts due to the high hydrophobicity of organic spacers, renders them practical applications in optoelectronic devices [58]. In addition, 2D perovskites with different diversity can be achieved through the incorporation of various bulky organic ligands, which ultimately showed tunable optical and electronic properties [59, 60]. Therefore, heterostructures incorporating distinct layered 2D perovskites with other layered or non-layered materials can also be easily realized, which exhibit unique optical and optoelectronic properties and vastly expand the potential functionalities and applications of the heterostructures [9, 61–64]. In this sense, summarizing the recent research progress on 2D perovskite-based heterostructures could facilitate the discovery of unexplored phenomena and open up a new range of optoelectronic applications.

Nevertheless, there are only a few review articles that have been reported regarding 2D perovskite-based heterostructures, focusing on either heterostructures based on 3D perovskite with 2D morphologies (e.g. $MAPbI_3$ films or nanoplatelets) [5] or Van der Waals heterostructures based on 2D Ruddlesden–Popper (RP) perovskites [62] or without including latest results [9], while the review concentrates on heterostructures based on 2D perovskites with both layered and non-layered materials such as Al_2O_3, 3D perovskites, and TMDs, is still lacking. To this end, it is urgent to summarize the recent progress of 2D perovskite-based heterostructures, covering more broad contents compared to previously reported ones and include the most updated research results, which can provide readers with more insight into 2D perovskite heterostructures. In this paper, we will review the recent achievements of 2D perovskite-based heterostructures. First, the structure and physical properties of 2D perovskites will be highlighted. The construction and characterizations of 2D perovskite-based heterostructures as well as the basic optical properties of the constructed heterostructures will then be illustrated. Furthermore, the potential applications of 2D perovskite-based heterostructures in photovoltaic devices, light-emitting diodes, photodetectors, phototransistors and

valleytronic devices will be demonstrated. Finally, we will summarize the current challenges and propose further research directions in the field of 2D perovskite-based heterostructures.

2. Structure and physical properties of 2D perovskites

2.1. Crystal structure of 2D perovskites

3D organic-inorganic halide perovskites (denoted as 3D perovskite hereafter) have a general formula of ABX_3, where A could be Cs or RNH_3, B can be Sn or Pb, and X can be Cl, Br or I [46, 65, 66]. Structurally 3D perovskites consist of BX_6 octahedrons which are connected at halogen atoms to form network structures. Small organic cations A are located at the void among octahedrons to stabilize the perovskite structure (figure 1(a)). 2D perovskites can be structurally considered as slicing 3D perovskites by inserting organic cation spacers among the BX_6 framework, leading to a natural quantum well structure with layered nature due to the fact that the adjacent inorganic layers are isolated by long-chain organic molecules and the interaction between inorganic layers are rather weak (figure 1(a)) [11, 47]. Depending on the type of cations inserted and the stacking arrangement between adjacent inorganic layers, 2D perovskites can be classified into RP phase [67] and Dion–Jacobson (DJ) phase [68] (figure 1(b)). The RP phases with monovalent cations between inorganic octahedron layers show a staggered arrangement with the adjacent inorganic layers shifted concerning each other by half a unit cell while DJ phases with divalent cations have an eclipsed stacking inorganic layers [69]. Compared with RP phase perovskites, where the adjacent organic layers are connected via weak Van der Waals forces, the DJ phase perovskites only have one layer of the organic molecule and thus the interaction between the organic layer and inorganic layer is a hydrogen bond. As a result, DJ phase 2D perovskites exhibit better stability while RP phase perovskites are much easier to mechanically exfoliate in order to stack heterostructure [70]. Therefore, RP phase 2D perovskites are mostly studied in 2D perovskite-based heterostructures, and we will focus on RP phases in the rest of the paper.

The chemical formula of RP phase 2D perovskites is $(RNH_3)_2A_{n-1}M_nX_{3n+1}$, where R is a long organic chain, A stands for monovalent organic cation, M refers to metal cations, usually Pb or Sn, X stands for halide anion, and n refers to the number of MX_6 octahedral layers sandwiched between the organic molecular layers [45, 50, 67]. The inorganic MX_6 layers function as the 'wells' while the organic spacers serve as the 'barriers', resulting in multi-quantum well structures [71]. According to the number of the octahedral layers (named as the layer number n) sandwiched between adjacent organic layers, quasi-2D perovskites are formed (figure 1(c)). Since quantum confinement and dielectric confinement strongly depend on the layer number n, the optical and electronic properties of quasi-2D perovskites vary with the layer number n accordingly [60, 72–74], which will be discussed below.

2.2. Physical properties of 2D perovskites

2D perovskites can be regarded as a hybrid system of MX_6 octahedral layer and organic spacers, which thus exhibit great flexibility in physical properties. Benefiting from their multi-quantum well structure, the band structure of 2D perovskites can be efficiently modulated by changing the number of inorganic layers sandwiched between organic layers (corresponding to the layer number n value) [75]. As n value increases, the bandgap of 2D perovskites decreases due to the reduction of the quantum confinement (figure 2(a)) [72] which allows for electrons to migrate from the phase with a small n number to a high n number while holes migrate in opposite direction. This is in contrast with TMD materials, which evolve from direct bandgap to indirect bandgap semiconductors as their geometric thickness increases from monolayer to multilayer [76]. 2D perovskites are always direct bandgap semiconductors no matter what the geometric thickness is for a certain layer number n. Under such a case, since it is not necessary to be monolayer due to the direct bandgap nature of 2D perovskites, it greatly releases the difficulty to prepare heterostructures for emission devices, which requires the constituent materials to be direct band semiconductors. Besides, the band structure of 2D perovskites is also associated with the angle of the M–X–M bond, which is further related to the structure distortion of $[MX_6]$ octahedrons, causing the shift of valence band and conduction band, leading to bandgap variation.

The regulation of 2D perovskite electronic structure can also be achieved through composition engineering by substituting halide anions from Cl to Br or I, resulting in a decrease of bandgap [77]. While the onset energy of the absorption peak reduces with the size increase of organic cations, the opposite absorption onset energy trend appears when replacing the Pb^{2+} cation with the Sn^{2+} cation [78, 79]. By tuning each component in 2D perovskites, both absorption and emission peaks of 2D perovskites can be adjusted to cover the entire visible wavelength range from 400 to 800 nm.

Accompanying the layer number n-dependent bandgap change, the optical properties of 2D perovskites also vary accordingly. As the layer number increases, both PL and absorption peaks show a gradual redshift, corresponding to the reduction of bandgap (figures 2(b) and (c)) [80]. In combination with changing the halide compositions [60], the bandgap of 2D perovskites can be tuned in the entire visible wavelength range and even ultraviolet wavelength, which is useful for solar cells, LEDs, and photodetectors.

Another appealing feature of 2D perovskites is their large exciton binding energy. Because of the large dielectric constant difference between the organic layer and inorganic layer, the electronic screening effect is greatly reduced, leading to the dielectric confinement effect (figure 2(d)) [71]. As a result, the exciton binding energy in 2D perovskites is extremely large, on the order of several hundreds of meV. In addition, as the layer number n increases, the dielectric confinement effect also reduces, leading to a decrease in the exciton binding energy (figures 2(e) and (f)) [53]. A scaling law of exciton binding energy is successfully estimated to describe how the exciton binding energy evolves with the layer number n. In addition,

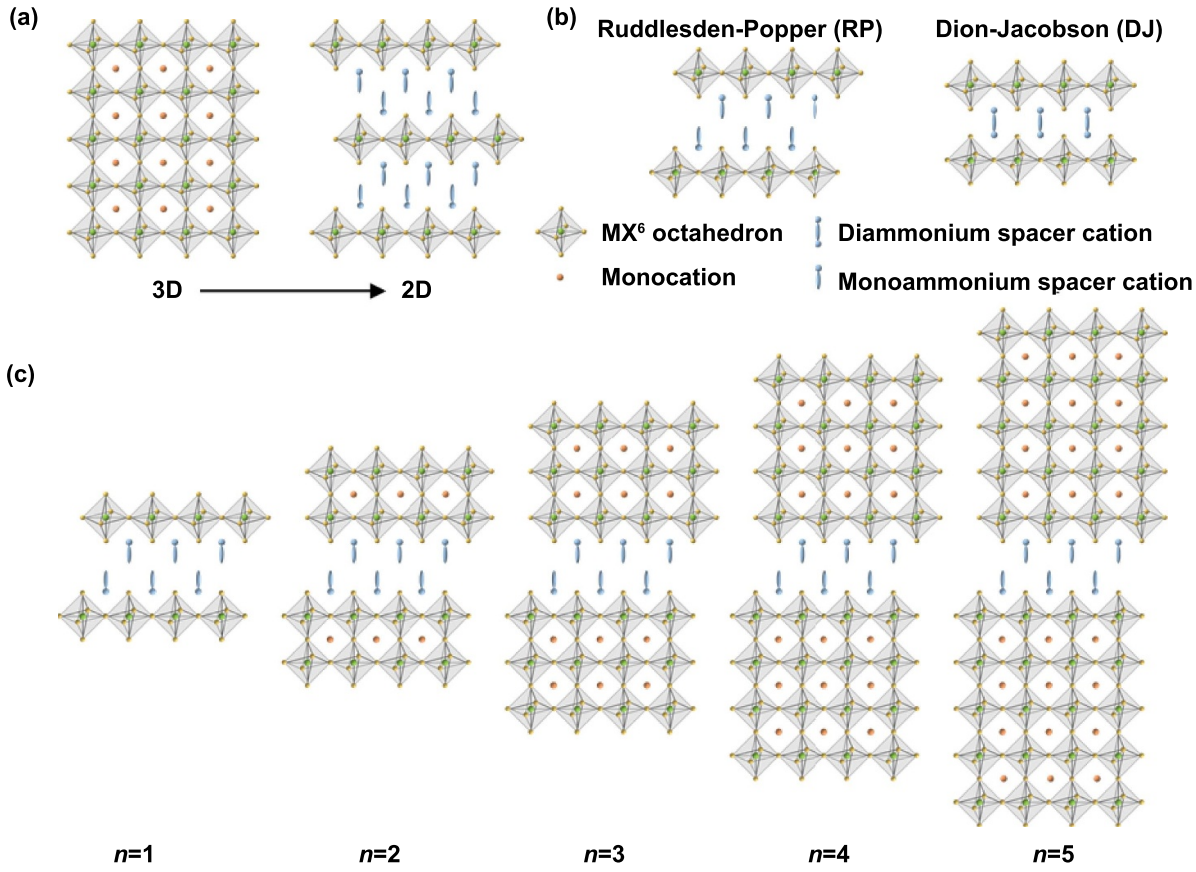

Figure 1. Schematic diagram of hybrid perovskites. (a) Schematic of perovskite from 3D to 2D structure. (b) Schematic of Ruddlesden–Popper (RP) phase and Dion–Jacobson (DJ) phase 2D perovskites. (c) Schematic of 2D RP phase perovskites with increasing layer number from $n = 1$ to $n = 5$.

benefiting from the multi-quantum well structure and large dielectric constant difference, a significantly large nonlinear optical effect has been observed in 2D perovskite crystals [81]. Strong two-photon induced emission has been demonstrated [82, 83] while strong biexciton emission has been achieved even under continuous wave laser excitation in 2D perovskite crystals [84].

Furthermore, the soft lattice nature and strong electron-phonon interaction in 2D perovskites lead to the formation of self-trapped excitons below the band edge, which gives rise to the strong broadband emission with a large Stokes shift [85–87]. The bandwidth of the self-trapped exciton emission is so broad that even white light emission can be achieved in 2D perovskites [88–90]. In addition, the self-trapped exciton emission in some 2D perovskites can be ascribed to the strong magnetic dipole transition, which provides a platform to explore strong magnetic dipole emission [91]. By using the weak absorption of self-trapped excitons below the band edge, the narrowband photodetector is achieved with a response range covering the whole visible range via tuning the layer number n and halide composition of 2D perovskites [92]. Importantly, the narrowband photodetector arrays have been also successfully demonstrated, which is capable of achieving narrowband imaging [93]. Besides, optical studies reveal that such self-trapped excitons also exhibit optical anisotropy, depending on the crystalline orientation of 2D perovskites [94]. Taking advantage of the optical anisotropy of self-trapped excitons, polarization-resolved narrowband photodetectors have been also fabricated with a decent performance [95].

The physical properties of 2D perovskites can also alter by incorporating long organic chains [59, 60]. In view of a wide choice of long organic chains, rich physics can be explored in 2D perovskites. First, although the electronic band structure of 2D perovskites is mainly determined by the inorganic layer, the electron-phonon interaction strength can be tuned via changing the organic molecules [59]. Therefore, self-trapped exciton emission is rather strong for some of 2D perovskites, whereas it is completely absent for part of other 2D perovskites. Second, since the dielectric constant varies significantly from molecule to molecule, the exciton binding energy in 2D perovskites also varies in a wide range, which would greatly affect the emission efficiency. Third, by replacing the long organic chains with chiral molecules, the chirality can be transferred from molecule to 2D perovskites, resulting in circularly polarized light emission and detection (figures 2(g) and (h)) [96], which would find important potential applications in spintronics and valleytronics.

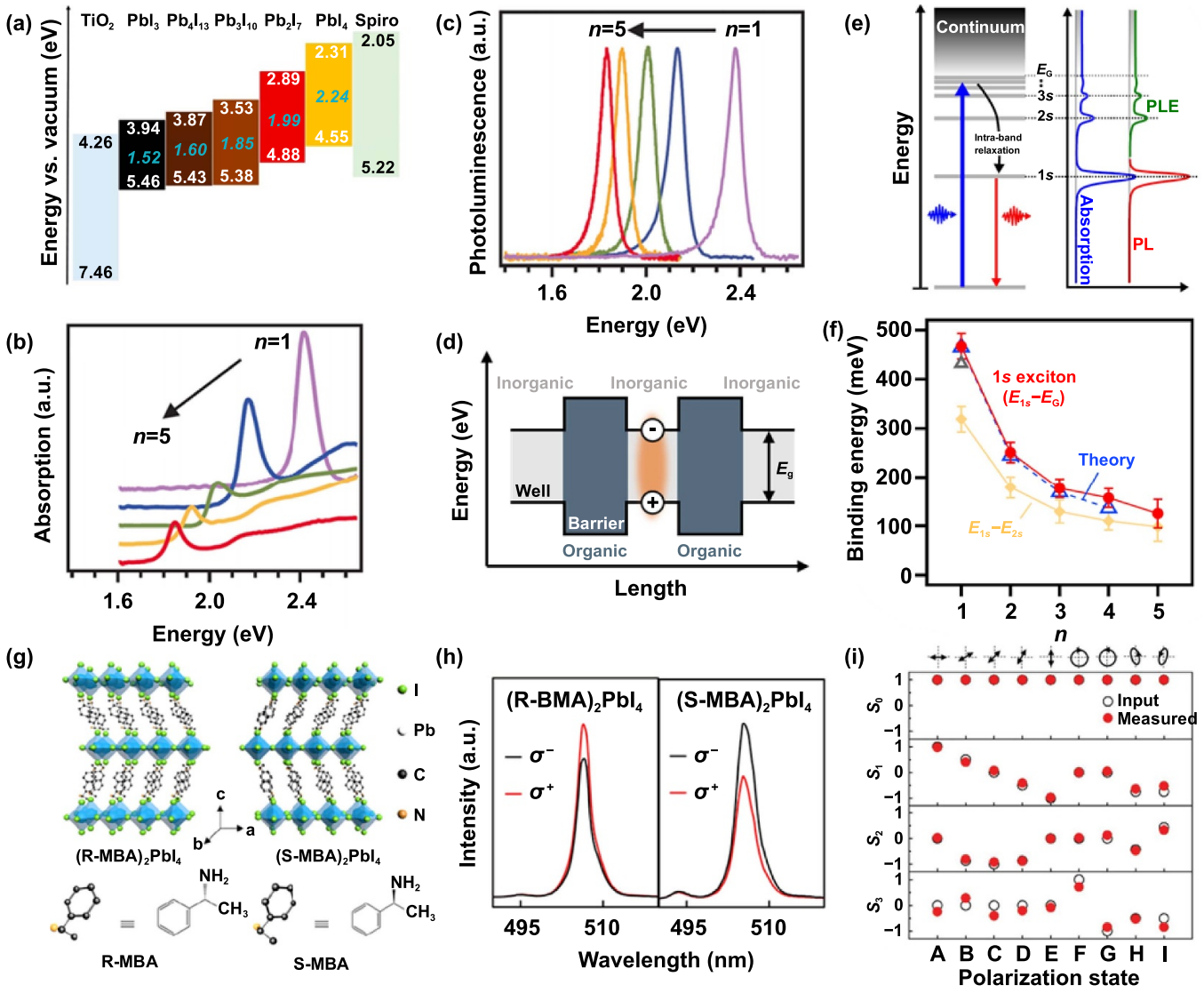

Figure 2. Optoelectronic properties of 2D perovskites. (a) Band alignment of the $(BA)_2(MA)_{n-1}Pb_nI_{3n+1}$ perovskite crystals with different layer number n. Reprinted with permission from [72]. Copyright (2015), American Chemistry Society. (b) Absorption and (c) PL of exfoliated $(BA)_2(MA)_{n-1}Pb_nI_{3n+1}$ perovskites with n from 1 to 5. From [80]. Reprinted with permission from AAAS. (d) Schematics of 2D quantum well structure in 2D perovskites. (e) Schematic of the Rydberg series of the exciton ground state (1 s) and excited exciton states (2 s, 3 s, etc) in 2D perovskite series and corresponding absorption, PL and PLE spectra typically observed in 2D perovskite series. (f) Exciton binding energy of experimental and theoretical results for $(BA)_2(MA)_{n-1}Pb_nI_{3n+1}$ perovskites with n from 1 to 5. Reprinted by permission from Springer Nature Customer Service Centre GmbH: Springer Nature, Nature Communications [53]. Copyright (2018). (g) Schematic of chiral 2D perovskites with opposite chirality. (h) Polarization-resolved PL spectra of chiral 2D perovskites. Reprinted with permission from [96]. Copyright (2019) American Chemistry Society. (i) Full-Stokes polarimeter based on $(R\text{-}MBA)_2PbI_4$ perovskites. [97]John Wiley & Sons.

Importantly, by taking advantage of the optical anisotropy between in-plane and out-of-plane direction and chirality introduced by the chiral organic molecule in chiral 2D perovskites, a full-Stokes polarimeter has been demonstrated (figure 2(i)) [97], which is capable of sensing all polarization states of incident light assisted by a theoretical model. Lastly, 2D perovskites could be equipped with ferroelectricity by properly selecting the organic cations and layer number n, which could be used to construct linearly-polarized light photodetectors.

To sum up, the rich physics offered by 2D perovskites renders them to be very promising for optoelectronic applications. Nevertheless, the presence of long organic chains in the out-of-plane would be detrimental for charge transport along this direction, leading to poor performance for solar cells and photodetectors. By properly controlling the growth direction so that the charge can transport along the in-plane direction, the PCE of 2D perovskite solar cells (PSCs) can be significantly improved [98]. In addition, although the insulating long organic chains are harmful to charge transport, exciton transport along the out-of-plane direction is still possible, which is beneficial to the room-temperature 2D perovskite-based exciton devices in view of the large exciton binding energy of 2D perovskites.

3. Construction and characterizations of 2D perovskite-based heterostructures

Heterostructure construction lays the foundation for optoelectronic device architectures and applications. Various techniques have been developed to build 2D perovskite heterostructures, which mainly include dry transfer, vapor deposition and solution synthesis. Through modulating materials and the stacking sequence integrated with 2D perovskites, heterostructures with different configurations can be obtained, which can not only expand the potential applications of optoelectronic devices, but also offer a stage for fundamental investigations.

3.1. Dry transfer

The layered nature of 2D perovskites enables us to obtain single or few layers of 2D perovskites by mechanical exfoliation from their bulk materials, which can be synthesized either by solution method or aqueous method [99]. With the subsequent dry transfer route, single/few-layer 2D perovskites can be integrated with other materials through layer stacking to form heterostructures [100, 101]. This technique was originally widely used for 2D materials, and is also applicable for 2D perovskites, a new member of the 2D material family. Due to the tunable layer number and organic chains of 2D perovskites, various types of heterostructures can be obtained. In a typical dry transfer process, samples can be transferred from one to the other substrate using polydimethylsiloxane (PDMS) stamps usually assisted by polymers including poly(methyl methacrylate) (PMMA) or poly(vinyl alcohol) (figure 3(a)) [100]. The PDMS stamp can be peeled off from the substrate due to the weak adhesion force between PDMS and samples while the polymer layer can be dissolved in the organic solvent. Since 2D perovskites are incompatible with most of organic solvents, we directly use a PDMS stamp without a polymer to transfer 2D perovskite microplates. After several cycles of the transfer processes, heterostructures with a designed stacking sequence can be achieved. Various 2D perovskites-based heterostructures, such as $(PEA)_2SnI_4/MoS_2$ ($PEA = C_6H_5C_2H_4NH_3$), $(BA)_2PbI_4/(BA)_2(MA)_2Pb_3I_{10}$ ($BA = C_4H_9NH_3$ and $MA = CH_3NH_{3TM}$) and (S- and R-MBA)$_2PbI_4/MoS_2$ ($MBA = C_6H_5C_2H_4NH_3$), has been recently demonstrated using this method [102]. Multiple layered heterostructures with good contacts and clean interfaces can be obtained with dry transfer routes. However, this method not only requires a tedious procedure, including mechanical exfoliation and cycles of transfer and alignment, but also requires post-annealing to remove the contaminant introduced by polymer stamps to realize efficient coupling between layers, leading to a low productivity and thus hindering large-scale applications.

3.2. Solution synthesis

Solution synthesis, which does not need tedious procedures and complicated equipment, is another technique to construct heterostructures at a low cost. Fu *et al* have demonstrated a solution method for fabricating $(PEA)_2(MA)_{n-1}Pb_nI_{3n+1}$ perovskites double and multilayer heterostructures. The time-resolved PL confirms the formation of heterostructures and suggests that the energy transfers from high- to low-energy bandgap induced by type I band alignment within hundreds of picoseconds. These heterostructures can emit multicolor light and thus provide potential platforms for optoelectronics, such as LEDs [103]. Another solution route for the fabrication of $(BA)_2PbI_4/(BA)_2(MA)Pb_2I_7$ heterostructures with tunable thickness and excellent crystal quality for narrow dual-band photodetectors also have been demonstrated by our group. (figures 3(b) and (c)) [104]. The basic principle for such growth is the different lattice constant, solubility, and growth rate between $(BA)_2PbI_4$ and $(BA)_2(MA)Pb_2I_7$.

Spin coating, a solution-based technique for the fabrication of 2D/3D perovskite heterostructure films to boost the stability of 3D perovskite-based solar cells, is also used for heterostructure fabrication. Through depositing each precursor with a predesignated sequence on the substrate by the spin coating method, heterostructures based on 2D perovskites can be realized. For instance, a precursor solution can be spin-coated on the previously peeled MoS_2 flakes to achieve $(PEA)_2PbI_4/MoS_2$ heterostructures [105]. Furthermore, epitaxial heterostructures can also be fabricated through the solution route. Dou's group has illustrated an ingenious strategy to achieve 2D perovskite epitaxial heterostructures in a quaternary solvent. This technique is applicable to different heterostructures via modulating metal cations, organic ligands, and halide sources [106].

3.3. Vapor deposition

The vapor deposition route was originally used for good-quality crystal or smooth film growth, which has become a predominant method for achieving heterostructures with scalability. Typically, volatile reactants are injected into the chamber under high temperatures, which causes the reactants to decompose or react with substances on the substrate, resulting in desired materials condensed onto the substrate. Vapor deposition has been widely used for 2D perovskites fabrication [107], which also have been demonstrated to form 2D perovskite-based heterostructures. Our group has demonstrated a strategy to obtain 2D perovskite-based $(BA)_2PbBr_4/(BA)_2MAPb_2Br_7$ heterostructures through the incorporation of solution synthesis with gas-solid phase intercalation (figure 3(d)) [108]. This strategy is also applicable for achieving both lateral and vertical $(BA)_2PbBr_4$/ $(BA)_2MAPb_2Br_7$ and $(PEA)_2PbI_4/(PEA)_2(MA)Pb_2I_7$ heterostructures, indicating its versatility. In addition, lateral heterostructures consisting of 2D perovskites $BA_2PbI_4/(BA)_2(MA)Pb_2I_7$ have also been presented with the vapor deposition method, in which PbI_2 films were first deposited through thermal evaporation and followed by organic vapor transport to form self-aligned lateral heterostructures. The as-prepared heterostructures exhibited potential applications for photodetectors [109]. Vapor deposition is favorable for achieving 2D perovskites with smooth surfaces suitable for optoelectronic devices. However, this

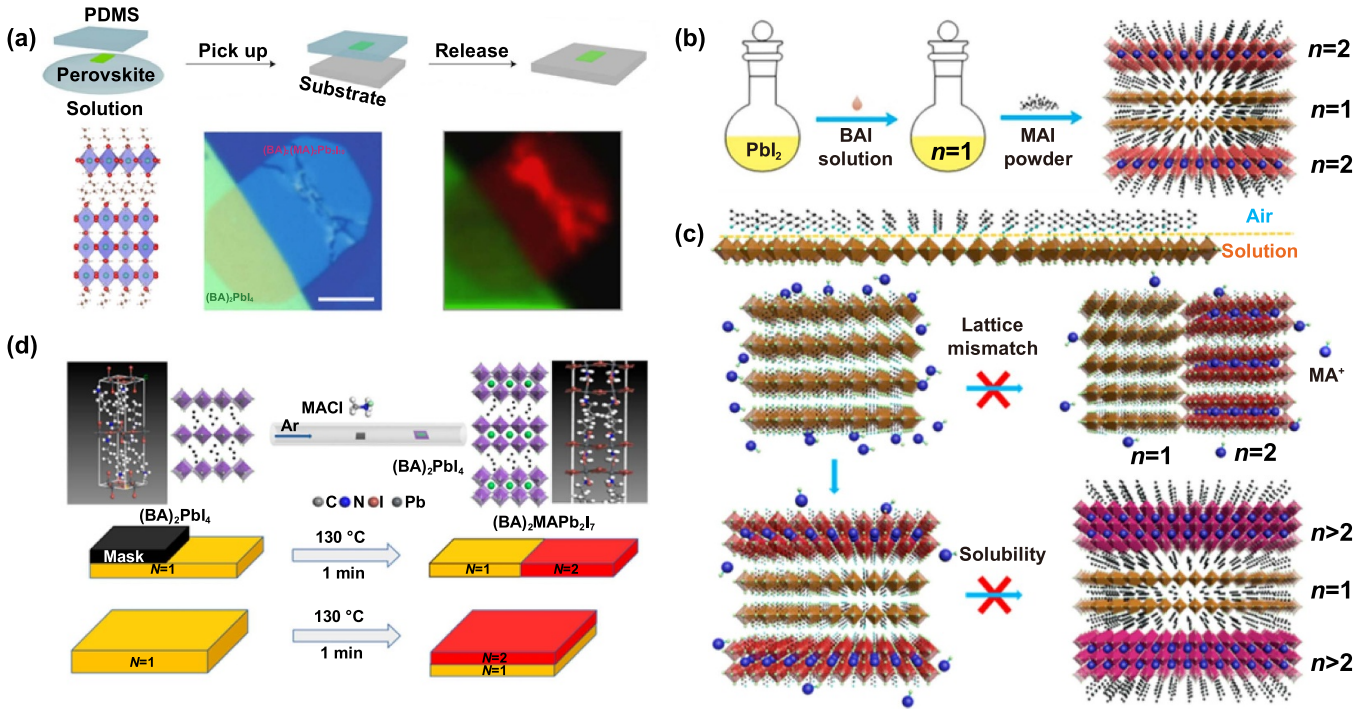

Figure 3. Construction of 2D perovskite-based heterostructures: (a) Dry transfer method. Reprinted by permission from Springer Nature Customer Service Centre GmbH: Springer Nature, Nature Nanotechnology [100], Copyright (2020). (b), (c) Solution synthetic method. Reprinted with permission from [104]. Copyright (2019) American Chemistry Society. (d) CVD and gas-solid phase intercalation synthetic method. Reprinted with permission from [108]. Copyright (2017) American Chemistry Society.

strategy requires unique instruments for reactions with high temperatures, such as chemical vapor deposition furnaces, leading to a complicated process with increased cost. Therefore, searching for energy-efficient techniques to synthesize 2D perovskite heterostructures is still an imperative topic and different suitable approaches are needed for optoelectronic devices with different applications.

Different types of 2D perovskite heterostructures can be obtained through the above synthetic methods. Van der Waals heterostructures can be obtained via mechanical exfoliation and the dry transfer route as well as the solution method while epitaxial heterostructures can be synthesized through solution synthesis method. In Van der Waals heterostructures, the lattice match is not stringently required and the layered nature of the constituent layers renders a high quality of the interface due to the free of dangling bonds at the surface of the constituent layers. In this sense, the Van der Waals heterostructures would exhibit better performance benefiting from the high-quality interface. In contrast, the lattice constants between the constituent layers should be stringently matched in order to achieve the formation of epitaxy heterostructures. In addition, defects and lattice distortions are usually present in epitaxy heterostructures, which would deteriorate the device performance.

3.4. Characterizations

Optical microscopy and optical spectroscopy including absorption and PL spectroscopy are the most used techniques to non-destructively characterize heterostructures, which have been also used to characterize 2D perovskites. Two materials in heterostructures can be distinguished from their colors in photographic pictures, reflecting the band gap of constituent components (figure 4(a)) [104]. For example, the as-synthesized centimeter-size $(BA)_2PbI_4/(BA)_2(MA)Pb_2I_7$ heterostructure crystals exhibit a red color corresponding to the color of $(BA)_2(MA)Pb_2I_7$ (left panel of figure 4(a)). Nevertheless, when we exfoliate the crystal using Scotch tape, the interior of the crystals shows a yellow color, corresponding to the color of $(BA)_2PbI_4$ (right panel of figure 4(a)). This observation clearly indicates the formation of the heterostructures. In addition, both absorption and PL spectra show the coexistence of peaks from $(BA)_2PbI_4$ and $(BA)_2(MA)Pb_2I_7$ in the heterostructures, revealing the presence of two different materials, while the interface of heterostructures cannot be examined (figure 4(b)) [104]. Therefore, spatially resolved PL mapping for the cross-section area among heterostructures can be used to verify the presence of the sharp interface and thus confirm the formation of heterostructures (figure 4(c)) [104]. However, the resolution of this strategy is limited by the spot size of excitation laser and the roughness of the cross-section of heterostructures, which gives poor resolution on the order of around 250 nm. To characterize the junction depth of the heterostructure more precisely, the reflection measurements have been carried out. Due to the refractive index difference between $(BA)_2PbI_4$ and $(BA)_2(MA)Pb_2I_7$, the reflection could take place at the interface. The reflected light from the interface will interfere with the reflected light from top surface of the heterostructures provided that both the interface and top surface are rather smooth, resulting in the interference pattern

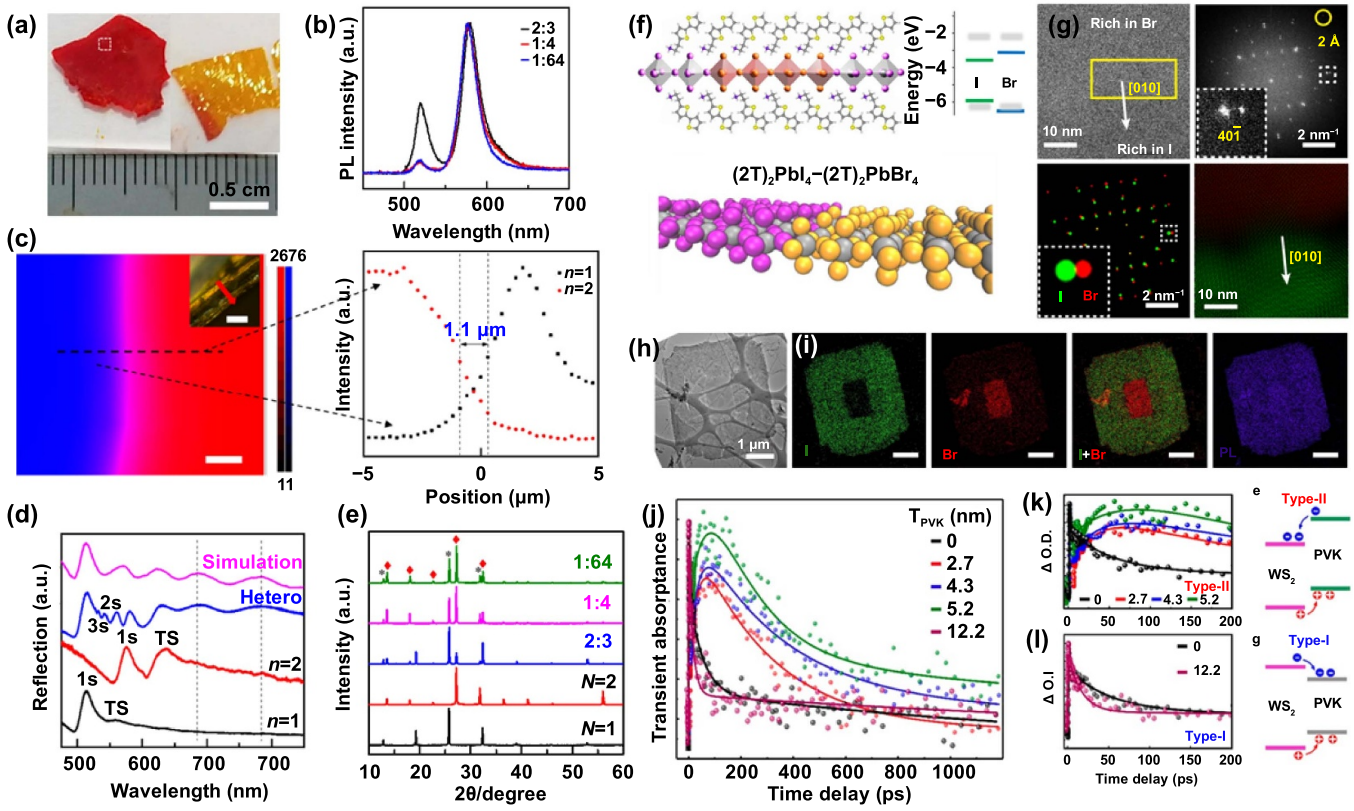

Figure 4. Characterizations of 2D perovskite-based heterostructures. (a) Optical image of $(BA)_2PbI_4/(BA)_2(MA)Pb_2I_7$ heterostructure. (b) PL spectra of $(BA)_2PbI_4/(BA)_2(MA)Pb_2I_7$ heterostructure with different mass ratios of BAI/MAI. (c) Cross-section PL mapping of $(BA)_2PbI_4/(BA)_2(MA)Pb_2I_7$ heterostructure and its PL intensity profile along the black dashed line. (d) Reflection spectra of $(BA)_2PbI_4$, $(BA)_2$ $(MA)Pb_2I_7$, and $(BA)_2PbI_4/(BA)_2(MA)Pb_2I_7$ heterostructure. (e) XRD patterns of $(BA)_2PbI_4$, $(BA)_2(MA)Pb_2I_7$, and $(BA)_2PbI_4/(BA)_2(MA)Pb_2I_7$ heterostructure with different mass ratios of BAI/MAI. Reprinted with permission from [104]. Copyright (2019) American Chemistry Society. (f) Schematic illustrations and band alignment of the $(2T)_2PbI_4/(2T)_2PbBr_4$ heterostructure. (g) AC-HRTEM and Fourier analysis of the $(2T)_2PbI_4/(2T)_2PbBr_4$ heterostructure. (h), (i) TEM image and EDS elemental mappings of the $(2T)_2PbI_4/(2T)_2PbBr_4$ heterostructure. Scale bars: 1 μm. Reprinted by permission from Springer Nature Customer Service Centre GmbH: Springer Nature, Nature [106], Copyright (2020). (j)–(l) Time-resolved pump-probe measurements of $(MA)_{n+1}Pb_nI_{3n+1}/WS_2$ heterostructure with different perovskite thickness. Reprinted with permission from [113]. Copyright (2019) American Chemistry Society.

in the reflection spectrum (figure 4(d)) [104]. Therefore, the junction depth can be estimated from interference pattern combined with the theoretical simulation. By using this technique, the junction depth of the as-synthesized heterostructure can be estimated to be below 100 nm.

The conventionally used characterization techniques, including X-ray diffraction (XRD) for phase identification, scanning electron microscopy (SEM), atomic force microscopy (AFM), and transmission electron microscopy (TEM) for surface morphology and topography adopted to characterize 2D perovskites are also applicable for 2D perovskite-based heterostructures. The XRD pattern can prove the existence of two constituent materials from the diffraction peaks but cannot provide information on the interface (figure 4(e)) [67, 104]. The structural feature of heterostructures can be reflected through the surface topography examination but these techniques cannot be used to validate the formation of heterostructures and study the interface property. Therefore, cross-sectional TEM would be a more efficient technique to directly investigate the interface among heterostructures (figures 4(f) and (g)) [106]. However, it is very challenging to carry out cross-sectional TEM since heterostructures usually grew on substrates, which makes it difficult to prepare samples for cross-section TEM. Besides, the decomposition of 2D perovskites when exposed to electron beams during measurements, causes inaccurate results [110]. To tackle this problem, heterostructures are grown on PMMA-covered substrates. When PMMA is dissolved in certain organic solvents, heterostructures can be obtained for further cross-sectional TEM measurement. Furthermore, to capture accurate TEM images for the heterostructure interface, the incident electron beam was shined to the nearby area of the target, leading to less structural damage [106]. Combined with EDS, the element distribution of the heterostructures can also be identified (figure 4(h)) [106].

Lastly, transient absorption spectroscopy also provides an efficient way to examine the heterostructures by studying the charge transfer [111] and energy transfer [112]. Once heterostructures are formed, the band alignment between constituent materials would inevitably lead to the charge transfer or/and energy transfer, which usually takes place in a very short timescale. Thus, transient absorption spectroscopy can

be used to prove such transfer process, which can further provide the band alignment information of the heterostructures. For instance, Pan's group has adopted transient absorption spectroscopy to investigate the band alignment in WS_2/2D perovskites with different thicknesses and identified that band alignment evolves from type-II to type-I as the thickness of 2D perovskites varies (figures 4(i)–(k)) [113]. Nevertheless, transient absorption spectroscopy cannot provide information on junction depth and interface of heterostructures either.

4. Optical properties of 2D perovskite-based heterostructures

Optical properterties are a fascinating functional aspect of 2D perovskite-based heterostructures, which not only inherit the basic physical properties of 2D perovskites but also show rich new photophysics that does not exhibit in each constituent material. Thus, 2D perovskite-based heterostructures provide an ideal platform to study rich charge-, energy-transfer and ion migration-induced optical properties and nonlinear optical effects.

Due to the different electronic band structures of 2D perovskites with different layer numbers n, type-II band alignment would usually form in heterostructures stacked by different 2D perovskites [100, 101]. Those 2D perovskite/2D perovskite heterostructures exhibit quenched emission for each constituent component arising from charge transfer, which is detrimental to emission devices. Nevertheless, the charge transfer among heterostructures is beneficial for photodetectors and solar cells. When the constituent 2D perovskite crystals have different halide elements, the halide ion migration would occur under thermal annealing, which is manifested by the emergence of an intermediate green emission peak (figures 5(a) and (b)) [101]. Based on the intensity of the intermediate green emission peak and theoretical model, the ion diffusion coefficients have been extracted.

Type II band alignment of 2D perovskite/monolayer TMD heterostructures also causes charge transfer across the interface within heterostructure, leading to some unique optical properties. Previous study revealed that PL intensity of the double-layer WS_2 can be greatly enhanced in double-layer WS_2/$(BA)_2(MA)_3Pb_4I_{13}$ heterostructure due to the local electric field induced by the oriented dipole moment at the interface originated from charge transfer (figures 5(c) and (d)) [114]. In addition, the air stability of $(BA)_2(MA)_3Pb_4I_{13}$ is also greatly improved in such a heterostructure. Charge transfer in the 2D perovskite/monolayer TMD heterostructures can also lead to the formation of interlayer excitons, which has been demonstrated by our group [115]. In such heterostructures, robust interlayer exciton emission can be easily observed without considering the twist angle and post-thermal annealing, which are usually required in monolayer TMD-based heterostructures so that strong interlayer coupling can be achieved. Therefore, this greatly simplifies the fabrication process for observing the interlayer exciton emission in 2D perovskite/TMD heterostructures. Furthermore, by varying the n value of 2D perovskite and the layer number of monolayer TMD, the interlayer exciton emission covers the visible to the near-infrared range, which facilitates the realization of broad-spectrum optoelectronics [116]. Importantly, by replacing the constituent 2D perovskites with chiral 2D perovskite, the valley degree of freedom can be efficiently tuned, which will be discussed in detail below [117]. In addition, Förster type energy transfer has been observed in WS_2/$(PEA)_2PbI_4$ heterostructures via fluorescence and PL excitation spectroscopy (figures 5(e) and (f)) [118].

In addition to 2D perovskite/TMD heterostructures, 2D perovskite/BP heterostructures have also been theoretically investigated [119, 120]. Both type-I and type-II band alignment are predicted in 2D perovskite/BP heterostructures relying on the metal element in 2D perovskites. In addition, under the external electric field, it is predicted that the band gap can be tuned and a phase transition from semiconductor to metal would take place. Importantly, the light absorption coefficient in such heterostructures can be enhanced. All those factors are favorable for 2D perovskite/BP heterostructures to be applied in optoelectronic devices.

2D perovskite-based multi-heterostructures have also been constructed by combining the solution synthesis method and dry transfer technique. $(BA)_2PbI_4$/$(BA)_2(MA)_2Pb_3I_{10}$/$(BA)_2(MA)Pb_2I_7$ multi-heterostructures have been fabricated by the Jin group (figures 5(g) and (h)) [100]. PL spectra from different locations of the multi-heterostructure reveal the charge transfer direction and confirm the type-I band alignment among those 2D perovskites. Besides, circularly polarized photoluminescence (CPL) in achiral perovskites can be stimulated and manipulated through formation of van der Waals heterojunctions between chiral and achiral perovskites. Through tuning the chemical composition, operation temperature and excitation wavelength, the degree of CPL polarization for achiral perovskites can be flexibly modulated [121].

Nonlinear optics tackles the interaction between matter and light, the research on which can be traced back to the 1960s, when second harmonic generation was originally discovered [122]. The nonlinear optical effects would contribute to important applications in the field of all optical switching, optical parametric oscillation, and information process and storage [123, 124]. In view of the strong nonlinear optical effect in 2D perovskites themselves [125, 126], nonlinear optical effect is also expected to appear in 2D perovskite-based heterostructures accordingly. Nonlinear optical effect of 2D perovskite $(BA)_2PbI_4$/$(BA)_2(MA)Pb_2I_7$ heterostructures have also been investigated systematically (figures 5(i) and (j)) [83]. The two-photon-absorption coefficient obtained through intensity-scan measurement was found to be related to the thickness of the heterostructure, which is around 44 cm MW^{-1} for a 20 μm thick sample. It is anticipated that both the $(BA)_2(MA)Pb_2I_7$ layer with $\sim$1 μm thickness as well as the non-radiative energy transfer through two layers in heterostructures give rise to the strong nonlinearity, which could further leads to applications in photodetectors.

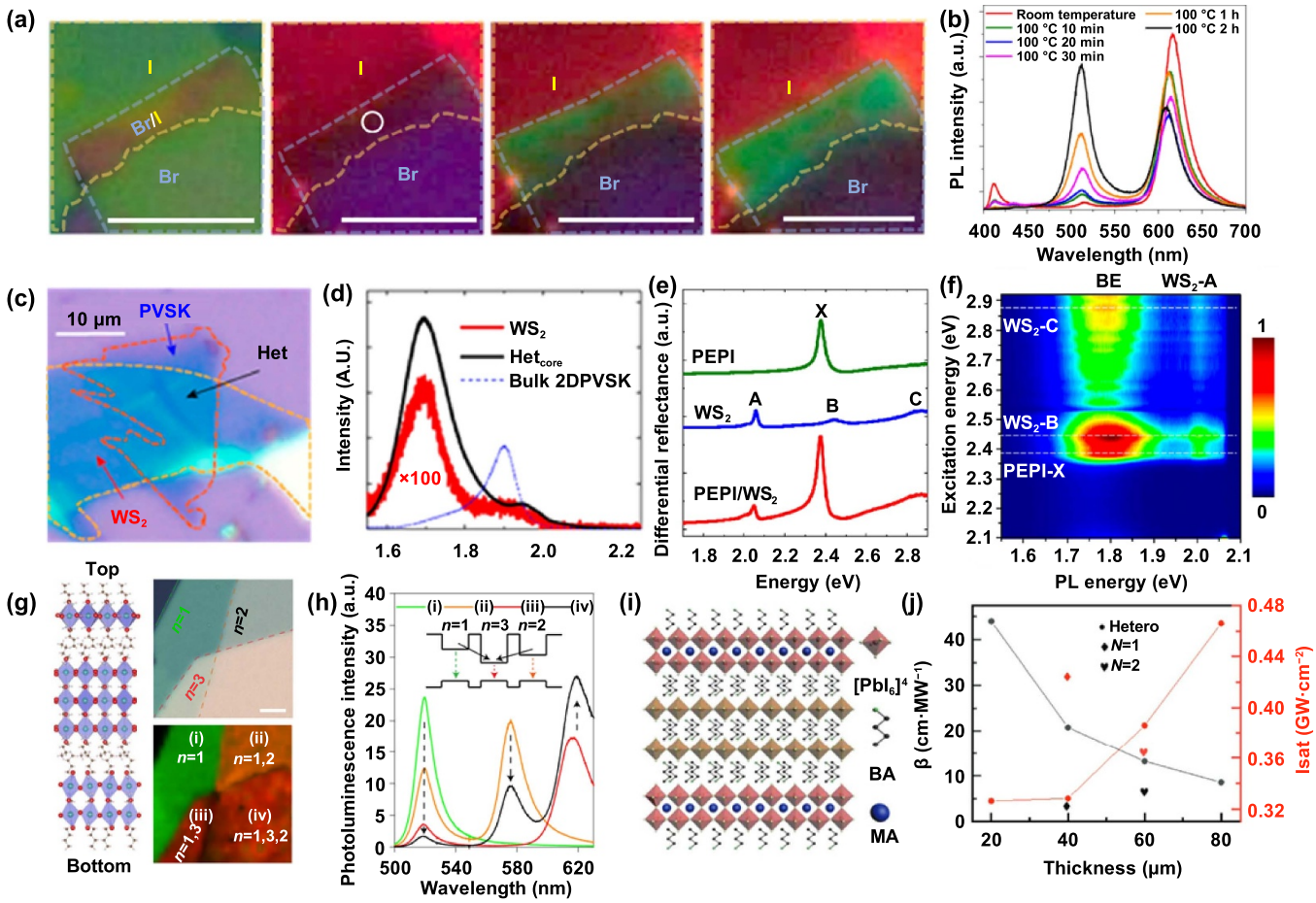

Figure 5. Optical properties of 2D perovskite-based heterostructures. (a) Bright-field image and PL images of $(BA)_2PbBr_4/(BA)_2(MA)_2Pb_3I_{10}$ vertical heterostructure heating at 60 °C for 1 and 8 h. (b) Evolution of PL spectra of $(BA)_2PbBr_4/(BA)_2(MA)_2Pb_3I_{10}$ heterostructure upon heating at 60 °C. Reprinted by permission from Springer Nature Customer Service Centre GmbH: Springer Nature, Nature Nanotechnology [101], Copyright (2021). (c) Optical image and (d) PL spectra of the 2 1 $WS_2/(BA)_2(MA)_3Pb_4I_{13}$ heterostructure. Reprinted with permission from [114]. Copyright (2019) American Chemistry Society. (e) Differential Reflectance spectra and (f) PLE spectra of the $(PEA)_2PbI_4/WS_2$ heterostructure. Reprinted with permission from [118]. Copyright (2020) American Chemistry Society. (g) Schematic of a $(BA)_2PbI_4/(BA)_2(MA)_2Pb_3I_{10}/(BA)_2(MA)Pb_2I_7$ multi-heterostructure and its corresponding optical image as well as PL mapping. Scale bar: 5 μm. (h) PL spectra collected in different regions in (g). The inset shows their band energy diagram and possible energy transfer processes. Reprinted by permission from Springer Nature Customer Service Centre GmbH: Springer Nature, Nature Nanotechnology [100], Copyright (2020). (i) Schematic of $(BA)_2PbI_4/(BA)_2(MA)Pb_2I_7$ heterostructure. (j) Thickness-dependent two-photon absorption coefficient and saturation intensity for $(BA)_2PbI_4/(BA)_2(MA)Pb_2I_7$ heterostructure. [83] John Wiley & Sons.

5. Optoelectronic applications of 2D perovskite-based heterostructures

2D perovskites can be stacked with other materials, such as TMDs, graphene, BP, 2D and 3D perovskite to establish heterostructures with different band alignments, which can be type I or type II based on different constituents in heterostructures [17]. In type-I heterostructures, carriers migrate from the large bandgap material to the smaller bandgap material while electrons and holes diffuse in opposite directions, leading to charge separation in type-II heterostructures. Therefore, different band alignments of heterostructures would lead to different optical and optoelectronic properties, and thus different optoelectronic applications. Generally, light-emitting devices require type-I heterostructures while type-II heterostructures would find important applications in photodetectors, solar cells and phototransistors.

5.1. Photovoltaic devices

In recent years, solar cells based on 2D/3D perovskite heterojunctions have attracted rising attention compared to single 3D perovskites since they not only inherit the remarkable charge carrier capabilities of 3D perovskites, but also exhibit relatively better environmental stability [127]. Besides, defects at the grain boundaries within 3D perovskites can be passivated [128], which leads to fewer defect traps with less hole-electron recombination and thus more efficient and stable photovoltaic devices [129]. For example, p–n heterojunction creation in perovskites can be used as a strategy to enhance the charge

separation, thus leading to suppressed carrier recombination in PSCs. Wang *et al* have constructed a 2D/3D perovskite heterostructure to improve the PCE and stability of PSCs. The PCE in such heterostructure solar cells can sustain 80% of its initial value after 1000 h in air and close to 4000 h when encapsulated (figures 6(a) and (b)) [130]. The heterostructures cover the grain boundaries of 3D perovskite to half of the film thickness, which induces the defects passivation, leading to less charge recombination and improved PCE with a certified efficiency of 21.5% [131].

The photovoltaic effect also has been observed in $(PEA)_2PbI_4$ 2D perovskite/monolayer WS_2 heterostructures. A device with vertical structure has been fabricated (figure 6(c)) [132], in which each constituent at the interface was responsible for the photovoltaic effect and graphene was used as an electrical contact. An open circuit voltage of 0.57 V and a short circuit current of 41.6 nA have been observed (figure 6(d)) [132]. The device also functioned as a self-driven photodetector with a photoresponsivity of 24.2 μA W^{-1} and external quantum efficiency (EQE) of 5.7×10^{-5}.

In addition, photon energy upconversion has been adopted to boost the efficiency of traditional photovoltaic devices to avoid the limitation of photon transmission loss with energies below the bandgap of channel semiconductors. The upconversion photovoltaic effect of $(PEA)_2PbI_4$ 2D perovskite/monolayer WS_2 heterostructures has been demonstrated by the Wee group (figures 6(e) and (f)), which is attributed to the below-bandgap two-photon absorption. The as-prepared devices showed an open circuit voltage of 0.37 V and short circuit current of 7.4 pA with a photoresponsivity of 771 pA W^{-1} and current on/off ratio of 130:1, indicating that the upconversion effect is a promising alternative to enhance the solar cell efficiency [133].

Generally, 2D perovskites are not ideal materials for solar cells since the long organic chains work as an insulating barrier which could hinder the charge transport. As a result, the PCE of 2D PSCs is lower than that of 3D PSCs. By stacking 2D perovskite with other materials to form heterostructures, 2D perovskite heterostructure solar cells can have both improved PCE and better environmental stability. The summary of the 2D perovskite heterostructure solar cells can be found in table 1. It is clear that the highest PCE for 2D perovskite heterostructure solar cells is still lower than that of 3D counterparts and further investigations are still required to improve the PCE.

5.2. Photodetectors

2D perovskite heterostructures-based optoelectronic devices are promising for photodetection since the dark current can be efficiently suppressed due to the formation of a built-in electrical field [134], and the photovoltaic effect stemmed from the built-in electric field among heterostructures also causes self-powered photodetection simultaneously, which is both sensitive and cost-effective [135, 136]. Various heterostructures based on 2D perovskite/graphene, 2D perovskite/2D perovskite, 2D perovskite/TMDs, and chiral 2D perovskites/TMDs have been constructed for light detection and imaging [102, 104, 108, 109, 137] while first-principles calculations have been used for studying the photodetection performance of 2D perovskites/BP heterostructures [119, 120]. Recently, van der Waals heterostructures combing chiral 2D perovskite ($(MBA)_2PbI_4$) with BP have been constructed with improved conductivity and thus have promoted performance of photodetectors based on these heterostructures [138]. Photodetectors composed of a 2D $(BA)_2PbBr_4$ crystal and monolayer graphene, which works as a source/drain as well as a perovskite protection layer, have been demonstrated (figure 7(a)) [137]. The spectral response shows a high responsivity of around 2100 A W^{-1}, benefiting from the large absorption coefficient of 2D perovskite and excellent charge collection efficiency by using graphene as contact. The photodetector exhibits a low dark current of $\sim 10^{-10}$ A and can sense light with wavelength above 520 nm (figure 7(b)) [137]. In addition, graphene/Au array/$(BA)_2(FA)_{n-1}Pb_nI_{3n+1}$ heterostructure photodetector shows a higher responsivity of 18.71 A W^{-1} compared with graphene/$(BA)_2(FA)_{n-1}Pb_nI_{3n+1}$ heterostructure photodetector and $(BA)_2(FA)_{n-1}Pb_nI_{3n+1}$ photodetector. In this case, both graphene and Au array facilitate carrier mobility and light absorption, thus significantly improving the performance of photodetector based on perovskites (figures 7(c) and (d)) [139].

2D perovskite/2D perovskite heterostructures are also good candidates for photodetectors due to their type-II energy band alignment. Centimeter-size $(BA)_2PbI_4/(BA)_2(MA)Pb_2I_7$ heterostructures with high purity and crystal quality, tunable thickness have been synthesized via solution route. This heterostructure-based photodetectors showed great potential for dual narrow band photodetectors, which delivered a low dark current of $\sim 10^{-12}$ A, high on–off ratio of $\sim 10^3$, and high spectral response with a full-width at half-maximum of 20 nm at 540 nm and 34 nm at 610 nm, which also can be ascribed to the self-trapping state assisted below-gap absorption (figures 7(e) and (f)) [104]. A sequential vapor deposition method has been also utilized to grow $(BA)_2PbI_4/(BA)_2(MA)Pb_2I_7$ heterostructures for photodetection. The photodetector shows an on-off ratio of 10^2 and a high responsivity of 8 A W^{-1}, which are attributed to the efficient photogenerated electron–hole separation under the built-in electric field (figures 7(g) and (h)) [109]. In particular, by using the strong nonlinear optical effect, 2D perovskite/2D perovskite heterostructures can also detect photons with energy smaller than their bandgap. For instance, a $(BA)_2PbI_4/(BA)_2(MA)Pb_2I_7$ heterostructure can sense 980 nm light with a responsivity of 10^{-7} A W^{-1}, taking advantage of the strong nonlinear optical effect of the heterostructure [83]. Lou's group also fabricated a $[(R)\text{-MPA}]_2MAPb_2I_7/MAPbI_3$ ((R)-MPA = (R)-methylphenethylamine) 2D/3D perovskite heterostructure photodetector, which can sense circularly polarized light. Under zero bias, the photodetector exhibits a remarkable anisotropy factor of 0.67, which is much larger than that in a $[(R)\text{-MPA}]_2MAPb_2I_7$ photodetector [140]. In particular, an X-ray detector has been also demonstrated based on $(FPEA)_2PbBr_4/FAPbBr_3$ heterostructure (FPEA = 4-fluorophenethylammonium; FA = formamidinium). The presence of a 2D perovskite layer can passivate the surface and

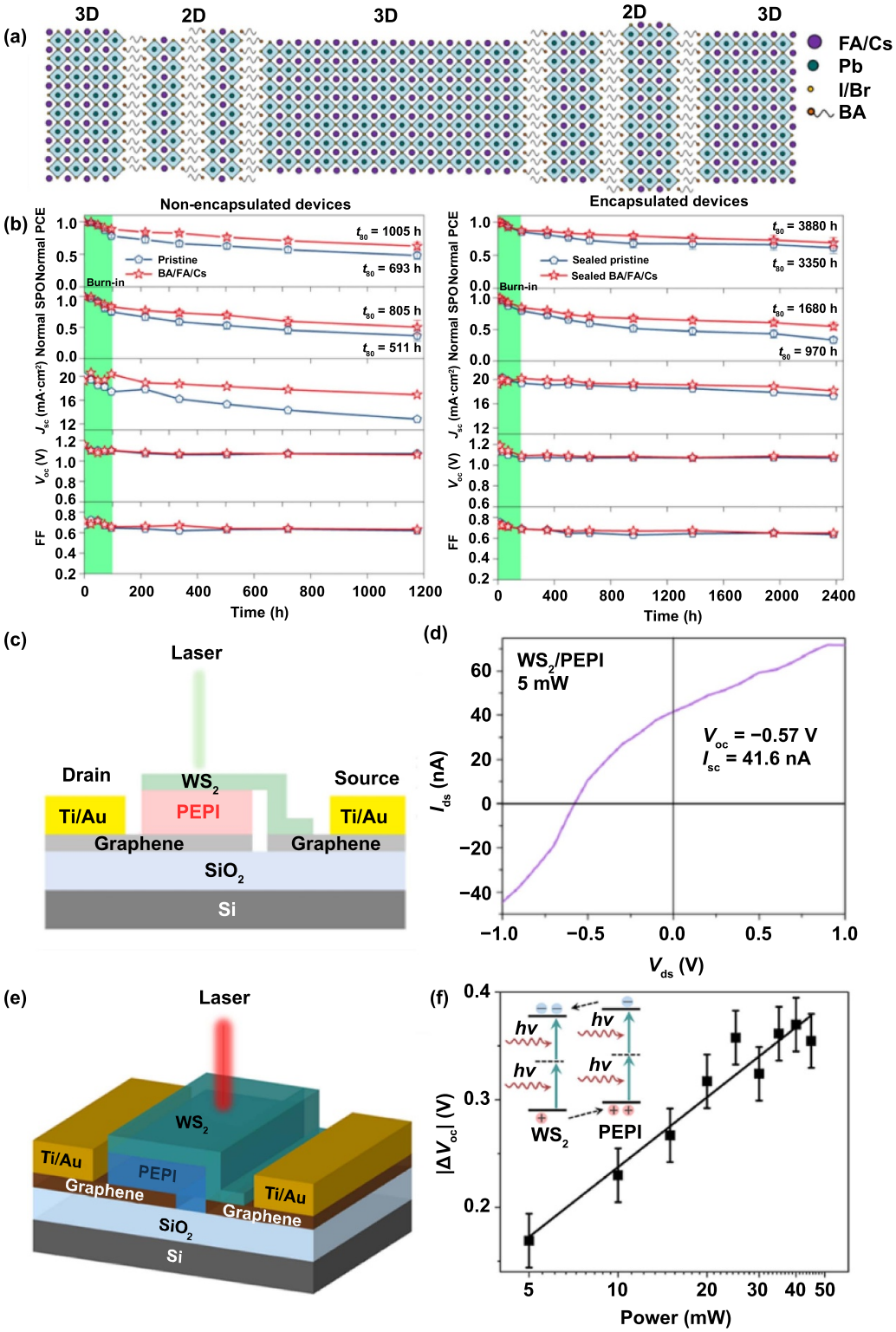

Figure 6. 2D perovskite-based heterostructure photovoltaic devices. (a) Schematic of self-assembled 2D–3D perovskite structure. (b) Comparison of device stability of non-encapsulated (left) and (right) encapsulated $FA_{0.83}Cs_{0.17}Pb(I_{0.6}Br_{0.4})_3$ (navy blue lines; labeled as pristine) and $BA_{0.09}(FA_{0.83}Cs_{0.17})_{0.91}Pb(I_{0.6}Br_{0.4})_3$ (red lines; labeled as BA/FA/Cs) perovskite solar cell devices. Reprinted by permission from Springer Nature Customer Service Centre GmbH: Springer Nature, Nature Energy [130], Copyright (2017). (c) Schematic of graphene/$(PEA)_2PbI_4$/WS_2/graphene heterostructure device. (d) $I_{ds} - V_{ds}$ characteristic of the heterostructure device under 5 mW laser exposure shows V_{oc} of −0.57 V and I_{sc} of 41.6 nA. Reprinted with permission from [132]. Copyright (2020) American Chemistry Society. (e) Schematic device structure of graphene/$(PEA)_2PbI_4$/WS_2/graphene heterostructure. (f) Upconversion photovoltaic effect of $(PEA)_2PbI_4$/WS_2 heterostructure and the shift of V_{oc} as a function of incident power. Reprinted with permission from [133]. Copyright (2021) American Chemistry Society.

Table 1. Photovoltaic devices of 2D perovskite-based heterostructures.

Structure	V_{OC} (V)	J_{sc} (nA)	J_{sc} density (mA cm^{-2})	PCE (%)	FF (%)	References
Graphene/WS_2 monolayer/$(PEA)_2PbI_4$/graphene	−0.57	41.6	—	—	—	[132]
Graphene/WS_2 monolayer/$(PEA)_2PbI_4$/graphene	0.37	7.4×10^{-3}	—	—	—	[133]
2D−3D (PEA,FA)SnI_3	0.47		20.07	6.98	74	[174]
$Cs_{0.17}(FA)_{0.83}Pb(I_{0.6}Br_{0.4})_3$	1.31		<20	19.4	78	[175]
$(PEA)_2PbI_4$/MAPI/$(PEA)_2PbI_4$	1.05		20.6	14.3	66	[176]
$(BA)_2PbI_4$/$MAPbI_3$	1.11		22.49	19.56	78	[177]
$(EDBEPbI4)_{0.03}[Cs_{0.05}$ $(FA_{0.83}MA_{0.17})_{0.95}$ $Pb(I_{0.83}Br_{0.17})_3]_{0.97}$	1.13		23.53	21.06	79.2	[178]
$MAPbI_3/(BA)_2(MA)_{n-1}Pb_nI_{3n+1}$	1.03		20.07	13.15	63.6	[179]
$(SBLC)_2PbI_4$/$MAPbI_3$	1.19		22.36	20.14	75.7	[180]
$(HOOC(CH_2)_4NH_3)_2PbI_4$/$MAPbI_3$	1.025		18.84	14.6	75.5	[181]
CA_2PbI_4/$MAPbI_xCl_{3-x}$	0.92		19.29	13.86	77.26	[182]
MAPI/PEAMAPI	1.08		18.63	14.94	73	[183]
$BA_{0.05}(FA_{0.83}Cs_{0.17})_{0.91}$ $Pb(I_{0.8}Br_{0.2})_3$	1.14		22.7	20.6	80	[130]

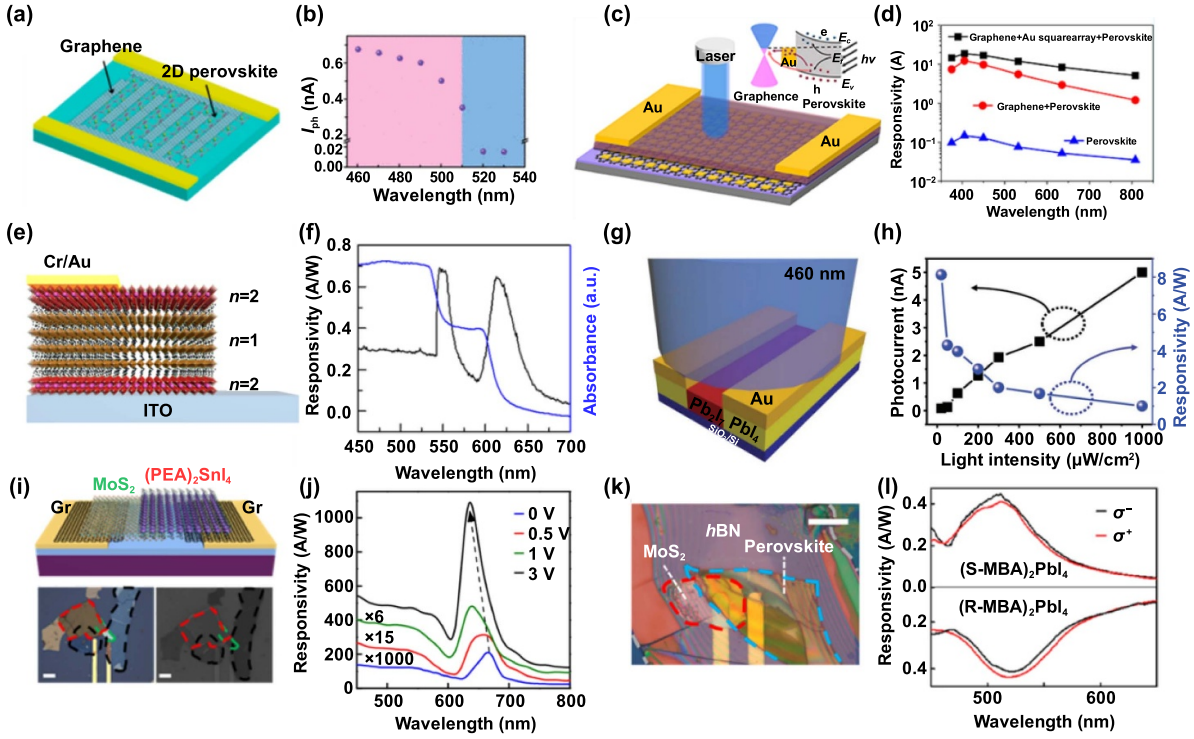

Figure 7. 2D perovskite-based heterostructure photodetectors. (a) Schematic of the $(BA)_2PbBr_4$ photodetector with interdigital graphene electrodes. (b) Spectral response of the device. Reprinted with permission from [137]. Copyright (2016) American Chemistry Society. (c) Schematic of the graphene/Au square nanoarray/$(BA)_2(FA)_{n-1}Pb_nI_{3n+1}$ hybrid-structure photodetector. (d) Spectra response of three kinds of photodetector. Reprinted with permission from [139]. Copyright (2021) American Chemistry Society. (e) Schematic of $(BA)_2PbI_4/(BA)_2(MA)Pb_2I_7$ vertical heterostructure photodetector. (f) Dual-band responsivity and normalized absorbance as a function of incident wavelength. Reprinted with permission from [104]. Copyright (2019) American Chemistry Society. (g) Schematic of photodetector based on $(BA)_2PbI_4/(BA)_2(MA)Pb_2I_7$ lateral heterostructure. (h) Photocurrent and responsivity as a function of light intensity. [109] John Wiley & Sons. (i) Schematic and optical image of graphene/$(PEA)_2SnI_4/MoS_2$/graphene device. (j) Responsivity under various biases. Reprinted with permission from [102]. Copyright (2019) American Chemistry Society. (k) Schematic of *h*-BN/$(R\text{-}MBA)_2PbI_4/MoS_2$ heterostructure photodetector. (l) Spectra response of *h*-BN/$(R\text{-}/S\text{-}MBA)_2PbI_4/MoS_2$ heterostructures under left- and right-circularly polarized illumination. Reprinted with permission from [96]. Copyright (2019) American Chemistry Society.

reduce the ion migration, resulting in a detectable X-ray dose rate of 55 $nGy_{air}s^{-1}$ [141].

Besides, the presence of the rectification behavior in 2D perovskite/TMD heterostructures with type II alignment allows them applicable for photodetectors [102, 132]. Photodetectors based on the heterostructure of $(PEA)_2SnI_4$ 2D perovskite/few-layer MoS_2 have been reported, which can realize light detection with tunable photoresponse in a broad range from visible to near-infrared. (figures 7(i) and (j)). When graphene was used as an electrical contact, the performance of the photodetector would be further boosted, which achieved a higher responsivity of 1100 A W^{-1} under 3 V bias, a rising

Table 2. Performance of photodetectors based on 2D perovskite heterostructures.

Structure	R (A/W)	Detectivity (Jones)	EQE (%)	On/off ratio	References
(4-AMP)$(MA)_2Pb_3Br_{10}$/$MAPbBr_3$	1.5	3.8×10^{10}	—	10^5	[184]
(4-AMP)$(MA)_2Pb_3Br_{10}$/$MAPbBr_3$	1.19×10^{-3} (@0 V)	1.26×10^{12}	—	10^5	[185]
Graphene/$(PEA)_2SnI_4$/MoS_2/graphene	1100	8×10^9	38.2	10^2	[102]
Graphene/$(PEA)_2PbI_4$/WS_2/graphene	24.2×10^{-6}	—	5.7×10^{-5}	1500	[132]
Graphene/$(PEA)_2PbI_4$/WS_2/graphene	7.71×10^{-7}	—	—	130	[133]
$(BA)_2(MA)_2Pb_3I_{10}$/MoS_2	10^4	4×10^{10}	—	—	[151]
h-BN/(R/S-MBA)$_2PbI_4$/MoS_2	0.45	2.2×10^{11}	—	14	[96]
MoS_2/$(PEA)_2PbI_4$	16.8	1.06×10^{13}	3.3×10^3	10^5	[105]
MoS_2/$(BA)_2(MA)_3Pb_4I_{13}$	121	4.3×10^{14}	10^5	10^3	[143]
$(BA)_2PbI_4$/$(BA)_2MAPb_2I_7$	0.69 (0.65)	—	158 (132)	10^3	[104]
$(BA)_2PbI_4$/$(BA)_2MAPb_2I_7$	10^{-7}	—	—	—	[83]
$(BA)_2PbI_4$/$(BA)_2MAPb_2I_7$	8.12	1.5×10^{12}	1.5×10^3	$>10^2$	[109]
Graphene/$(PEA)_2PbI_4$/graphene	730	—	—	—	[172]
Graphene/$(BA)_2PbBr_4$/graphene	2100	—	—	10^3	[137]
Graphene/$(BA)_2FAPb_2I_7$	12.25	1.44×10^{13}	—	—	[139]
Graphene/Au array/$(BA)_2FAPb_2I_7$	18.71	2.21×10^{13}	—	6×10^4	[139]
Graphene/Au array/$(BA)_2PbI_4$	5.03	5.93×10^{12}	—	10^4	[139]

time of 40 ms under zero bias, as well as a rectification ratio of 500 [102]. Furthermore, benefiting from the selection flexibility of the organic chain in 2D perovskites, chirality can be easily introduced to 2D perovskites via the incorporation of chiral molecules [142], which are empowered with both chirality and the properties of perovskites and thus exhibit potential optoelectronics with new desirable functionalities. Heterostructures based on a *h*BN/Chiral 2D perovskite/MoS_2 heterojunction are capable of sensing circularly polarized light at room temperature (figures 7(k) and (i)) [96]. Furthermore, Xie's group demonstrated a sensitive and ultrafast sub-band-gap photodetector based on a $(BA)_2MA_3Pb_4I_{13}$/few-layer MoS_2 heterostructure, which exhibits a responsivity of 121 A W^{-1} and a detectivity of 4.3 $\times$ 10^{14} Jones under 860 nm laser excitation [143]. In particular, the photodetector shows a fast response time of microsecond. The high responsivity and fast response speed can be ascribed to the strong interlayer transition of sub-band-gap photons and the rapid separation of the photogenerated carriers due to the built-in field.

Taking the advantage of a large number of 2D perovskites and layered materials that can be selected to construct heterostructures, the performance of 2D perovskite-based heterostructure photodetectors is continuously improving (table 2). In addition to light intensity, the frequency and polarization states of incident light can also be sensed by properly selecting the stacking materials. Nevertheless, studies on 2D perovskite-based heterostructure photodetectors are still in their infancy and further investigations are required to explore more new functionalities and further improve their performance.

5.3. Light-emitting devices

2D perovskite-based heterostructures can also be adapted to realized light-emitting in view of the excellent rectification behavior and tunable energy band alignment. By using the layer number *n*-dependent electronic band structure, a type I band alignment is formed (figure 8(a)) [75]. With such alignment, the electrically injected electrons and holes will flow to the component with smallest band gap. As a result, the injected carrier recombination will occur in material with the smallest band gap, leading to the strong electroluminescence. This process is called energy funneling effect. Light emission efficiency can be greatly improved by using the energy funneling effect [144, 145], which has been demonstrated in $(PEA)_2(MA)_{n-1}Pb_nI_{3n+1}$ heterostructures with the highest EQE of 8% (figures 8(a)–(c)) [75].

Light-emitting diodes based on perovskite-polymer bulk heterostructures (PPBH) have also been demonstrated, in which the emissive layer is composed of 2D/3D perovskites and an insulating layer of poly(2-hydroxyethyl methacrylate) (figure 8(d)). The peak EQE of the best device can be up to 20.1% when current densities are within the range of 10^{-3}–0.1 mA cm^{-2}, setting a record for LEDs based on perovskites (figure 8(e)). When the epoxy adhesive/cover glass was used to encapsulate the devices, the half-life (T50) under continuous usage in air with a current density of 0.1 mA cm^{-2} corresponding to the EQE peak point can be 46 h (figure 8(f)) [146]. In addition, a 2D/3D perovskite heterostructure has been used to achieve a multi-functional photonic device, which can work as both a solar cell and an LED. This can be ascribed to the charge transfer across the interface, inducing increased carrier density and enhanced carrier recombination [147]. These results suggest the potential applications of perovskite heterostructures in LEDs.

Furthermore, electroluminescence from charge transfer excitons has been achieved in $(PEA)_2PbI_4$/$(PEA)_2SnI_4$ heterostructures. Due to the type II band alignment induced charge transfer between those 2D perovskites, the electrons and holes distribute in different components (figure 8(g)). Taking into account the Coulomb interaction between electrons and holes,

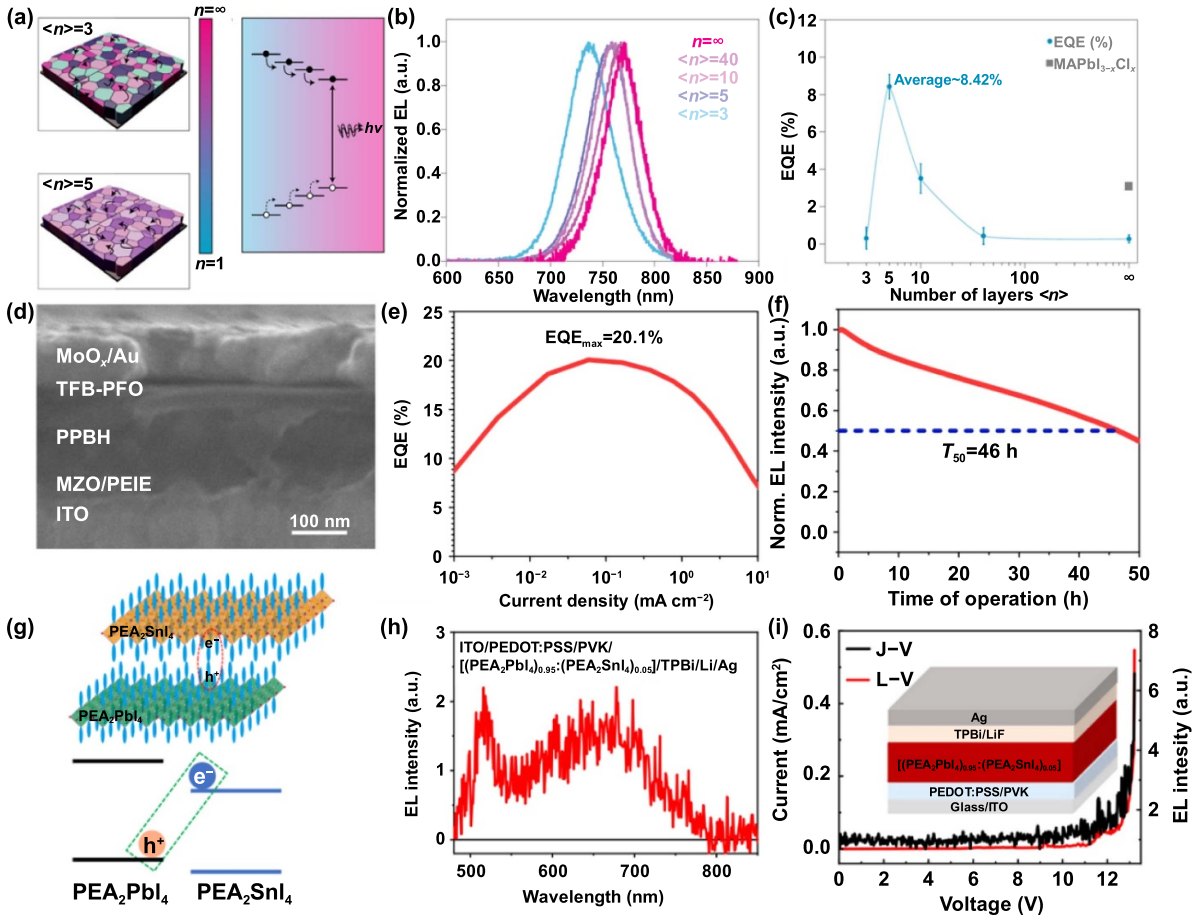

Figure 8. 2D perovskite-based heterostructure light emitting devices. (a) Schematic of carrier transfer in $(PEA)_2(MA)_2Pb_3I_{10}$ perovskite and $(PEA)_2(MA)_4Pb_5I_{16}$ perovskite (left) and energy funneling in multi-phase $(PEA)_2(MA)_{n-1}Pb_nI_{3n+1}$ perovskite to commit smallest bandgap emission (right). (b) Normalized EL spectra of $(PEA)_2(MA)_{n-1}Pb_nI_{3n+1}$ perovskite with different n values. (c) EQE comparison for $(PEA)_2(MA)_{n-1}Pb_nI_{3n+1}$ perovskite with different n values. Reprinted by permission from Springer Nature Customer Service Centre GmbH: Springer Nature, Nature Nanotechnology [75], Copyright (2016). (d) Cross-section SEM image of $(NMA)_2(FA)Pb_2I_7$-based LED structure. (e) EQE as a function of current density. (f) Stability performance at a constant current density of 0.1 mA cm^{-2} in the air for 50 h. Reprinted by permission from Springer Nature Customer Service Centre GmbH: Springer Nature, Nature Photonics [146], Copyright (2018). (g) Schematic of $(PEA)_2PbI_4/(PEA)_2SnI_4$ heterostructure and the formation of the charge-transfer exciton. (h) EL spectrum of $(PEA_2PbI_4)_{0.95}:(PEA_2SnI_4)_{0.05}$-based LED. (i) *I–V* and EL-V characteristics under electrical injection. Reprinted by permission from Springer Nature Customer Service Centre GmbH: Springer Nature, Nature Communications [148], Copyright (2020).

the charge transfer excitons are formed in a timescale of 3 ps. Those charge transfer excitons have a long lifetime of 0.5 μs and show a broad emission peak below the bandgap. In particular, such charge transfer excitons can also form via electrically injected carriers, leading to broadband electroluminescence (figures 8(h) and (i)) [148].

Although 2D perovskite-based heterostructures show promise in light-emitting devices, currently there are only a few reports on them. The limiting factors include the poor electrical conductivity of 2D perovskites and poor electrical contact between electrode and 2D perovskites. With further advancement of 2D perovskites, the intentionally orientated 2D perovskites can partially overcome the poor electrical conductivity of 2D perovskites while directly contacting 2D perovskites via metal electrode transfer might tackle the contact issue.

5.4. Phototransistors

2D perovskites-based heterostructures also can function as phototransistors. A phototransistor integrates the functions of the transistor and photodetector. The transistor can inherently amplify the signal while the photodetector can sense the incident light signal. As a result, the phototransistors are expected to have very high photoresponsivity and EQE, which make them promising for ultrasensitive light detection [149]. For instance, spin-coating strategy has been used to fabricate multiphase 2D perovskite/graphene heterostructures, leading to 2D perovskite being aligned and perpendicular to the substrate. The phototransistor showed a prompt photoresponse and a responsivity of $\sim 10^5$ A W^{-1} at 532 nm, which might be attributed to the spatial separation of electron–hole pairs facilitated by the bending energy band induced by the built-in

electric field [150]. Alternatively, the dry transfer method has also been adopted to fabricate 2D perovskite/MoS_2 and 2D perovskite/graphene heterostructures for phototransistors. In 2D perovskite/MoS_2 phototransistors, the photoresponse is improved by six orders of magnitude by stacking 2D perovskite microplates onto MoS_2 flake compared with that of bare 2D perovskite microplates. By applying a gate voltage, the dark current can be significantly suppressed without scarifying the overall performance (figures 9(a) and (b)) [151]. In addition, Loh's group has constructed $(BA)_2(MA)_3Pb_4I_{13}$/graphene heterostructures and studied the charge injection. Under light illumination, both electron and hole concentration drastically increases, resulting in the significant reduction of the conductance gap. As a consequence, the current under light illumination is significantly improved and less dependent on gate voltage applied (figures 9(c) and (d)) [152].

Besides, iodide loss has been revealed to be a degradation pathway for 2D perovskites through positively charged iodide vacancy generation in 2D perovskite/graphene heterostructures. With further covering graphene as an encapsulation layer, a phototransistor based on a graphene/2D perovskite/-graphene device structure has been demonstrated, in which the iodide loss has been suppressed with improved perovskite stability (figure 9(e)). In addition, such a heterostructure exhibited strong gate-dependent photoresponse under all excitation powers investigated (figure 9(f)) [153].

2D perovskite/Al_2O_3 heterostructure has been used as a dielectric for MoS_2 phototransistors (figure 9(g)). Type II band alignment within 2D perovskite/Al_2O_3 favors the photogenerated charge carrier separation, thus leading to high broadband photoresponse. Besides, the negligible hysteresis, caused by both ion migrations in perovskite and charge trapping in Al_2O_3, leads to phototransistors with low-voltage and enhanced bias stress stability. Furthermore, the external bias influences carrier recombination in 2D perovskites. With certain gate biases, the devices show wavelength-dependent photoresponsivity of 10^3–10^8 A W^{-1} regardless of incident light intensity (figure 9(h)) [154].

5.5. Valleytronic devices

Valleytronics refers to using valley degrees of freedom to manipulate and store information [155]. Monolayer TMDs provide an ideal platform to investigate valleytronic devices due to their spin-valley locking effect and thus have been extensively studied in the last decade [156–160]. It is crucial to efficiently manipulate the valley pseudospin for valley-associated applications. Although a number of strategies include circularly polarized light excitation [156] using strain field [161] and using proximity effect by stacking with magnetic substrate have been developed to control the valley polarization [42, 162], they either require complex optical systems or need very low temperatures and external magnetic fields, thus increasing the cost.

Taking advantage of spin-valley locking effect in monolayer TMDs, it is possible to manipulate the valley pseudospin via injecting spin-polarized carriers into monolayer TMDs [163]. Previous studies have demonstrated that spin polarization in Pb-based chiral 2D perovskites can reach over 80% and over 90% in Sn-based chiral 2D perovskites [164, 165]. Therefore, using chiral 2D perovskites as a spin source to inject spin-polarized carriers into monolayer TMDs would be an efficient route to manipulate the valley polarization of monolayer TMDs. Our group has successfully fabricated chiral 2D perovskite/monolayer MoS_2 heterostructures and demonstrated the efficient valley manipulation (figures 10(a)–(d)) [117]. By properly choosing chiral 2D perovskites with certain chirality, the spin-polarized carriers can be selectively injected into K or K′ valley, resulting in different valley polarization of monolayer MoS_2 under linearly polarized light excitation (figure 10(d)). The average spin injection efficiency is estimated to be around 78% at 77 K. By using this method, the manipulation of valley polarization via chiral 2D perovskites still validates up to 200 K, which is of great importance for high-temperature valleytronic devices.

Although the manipulation of valley polarization can be achieved for free excitons in chiral 2D perovskite/monolayer MoS_2 heterostructures, the lifetime of free excitons in monolayer MoS_2 is rather short, which is detrimental to valleytronic devices [166, 167]. Interlayer excitons, in which the constituent electrons and holes are spatially separated, would have a longer lifetime and thus be favorable for valleytronics [168, 169]. Similar to monolayer TMD heterostructures, interlayer excitons can be also formed in 2D perovskites-based heterostructures. Interlayer coupling has been observed in 2D perovskites/monolayer TMD heterostructures (figures 10(e) and (f)) [115]. The twist angle among layers influences the interlayer excitons formation in TMD heterostructures and thermal annealing is usually used to achieve strong interlayer exciton emission [170]. While for 2D perovskites/monolayer TMDs heterostructures, the interlayer coupling can be robustly formed without considering the rotation angle and thermal annealing, which makes the fabrication process much easier. In addition, the interlayer exciton emission intensity in 2D perovskite/monolayer TMDs heterostructures can be readily controlled via external strain, providing another degree of freedom to tune the interlayer coupling strength [171]. Importantly, those interlayer excitons also exhibit circularly polarized light emission in chiral 2D perovskite/WSe_2 heterostructures under linearly polarized light excitation, suggesting that the valley polarization persists for interlayer excitons. Therefore, chiral 2D perovskites can be also used to control the valley polarization of interlayer excitons in 2D perovskite/monolayer TMD heterostructures. A degree of circularly polarized light emission for interlayer excitons can reach 13% at 77 K in chiral 2D perovskite/monolayer WSe_2 heterostructure, indicating its potential for valleytronic devices.

In addition to the above-mentioned applications, optical synapses based on 2D perovskite/graphene heterostructures also have been demonstrated with a high photo responsivity and excellent stability up to 74 days [172]. The optical synapse can realize reconfigurable light-evoked excitatory/inhibitory functions and achieve direct pattern recognition with an accuracy of 80%. Besides, a 2D perovskite/carbon nanotube transistor has been fabricated, which exhibits

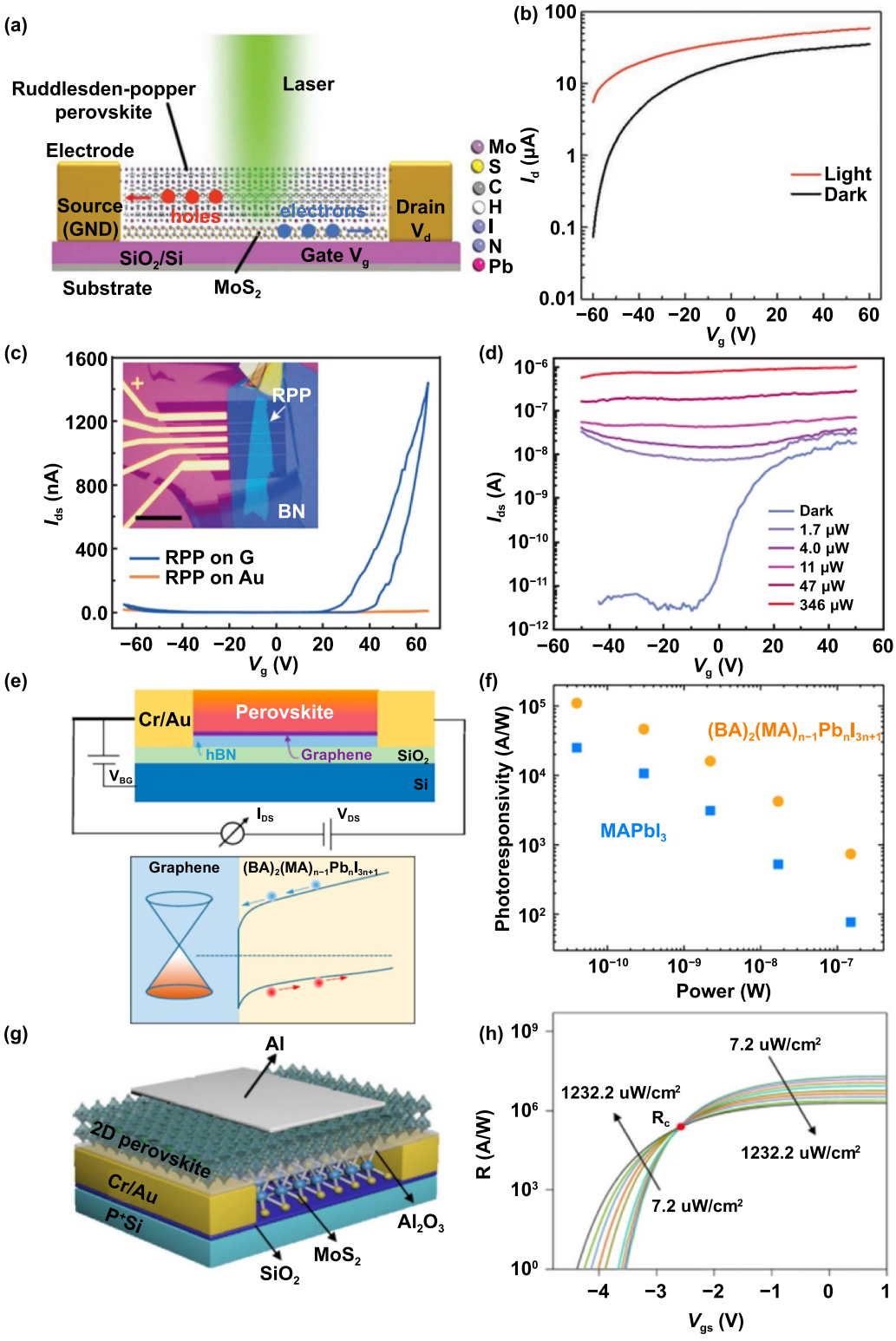

Figure 9. 2D perovskite-based heterostructure phototransistor. (a) Schematic of $(BA)_2(MA)_2Pb_3I_{10}/MoS_2$ hybrid phototransistor. (b) $I_d - V_g$ curves under dark and light conditions. [151] John Wiley & Sons. (c) Transfer characteristics and optical image of $(BA)_2(MA)_3Pb_4I_{13}$/graphene and $(BA)_2(MA)_3Pb_4I_{13}$/Au FET device at 1.7 K. (d) Transfer characteristics in dark and under illumination with different intensity for $(BA)_2(MA)_3Pb_4I_{13}$/graphene device at 77 K. Reprinted by permission from Springer Nature Customer Service Centre GmbH: Springer Nature, Nature Communications [152], Copyright (2020). (e) Schematic of mechanism of $(PEA)_2PbI_4$/graphene heterostructure phototransistor. (f) Photoresponsivity of graphene/$(PEA)_2PbI_4$/graphene phototransistor as a function of voltage and incident power. Reprinted from [153], Copyright (2018), with permission from Elsevier. (g) Schematic of $MoS_2/Al_2O_3/(PEA)_2(MA)_2Pb_3I_{10}$ hybrid phototransistor. (h) Photoresponsivity dependence of gate voltage and illumination intensity. Reprinted by permission from Springer Nature Customer Service Centre GmbH: Springer Nature, Nature Communications [154], Copyright (2020).

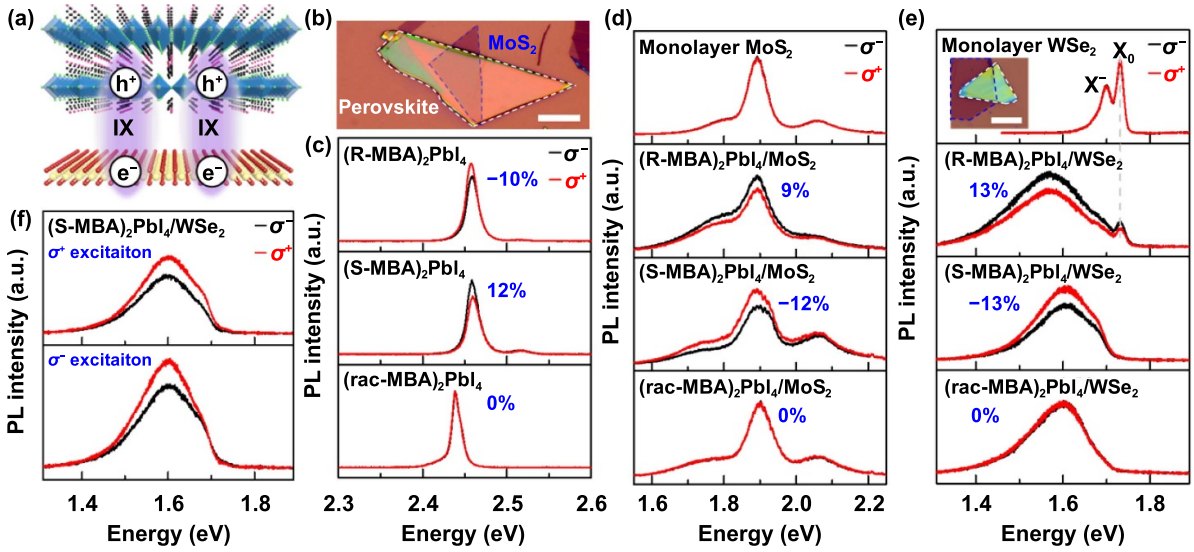

Figure 10. Valleytronic devices of 2D perovskite-based heterostructures. (a) Schematic of 2D perovskite/monolayer TMD structure and the formation of interlayer excitons. (b) Optical image of chiral 2D perovskite/monolayer MoS_2 heterostructure. Scale bar: 10 μm. (c) Polarization-resolved PL spectra of (R-/S-/rac-MBA)$_2$PbI$_4$ flakes under linearly polarized 473 nm laser excitation. (d) Polarization-resolved PL spectra of individual monolayer MoS_2 and (R-/S-/rac-MBA)$_2$PbI$_4$/monolayer MoS_2 heterostructures under linearly polarized 532 nm laser excitation. (e) Polarization-resolved PL spectra of individual monolayer WSe_2 and (R-/S-/rac-MBA)$_2$PbI$_4$/monolayer WSe_2 heterostructures under linearly polarized 633 nm laser excitation. Reprinted with permission from [117]. Copyright (2020) American Chemistry Society. (f) Polarization-resolved PL spectra of a (S-MBA)$_2$PbI$_4$/monolayer WSe_2 heterostructure under left- and right-circularly polarized 633 nm laser excitation. Reprinted with permission from [115]. Copyright (2020) American Chemistry Society.

multilevel optical memory function via tuning the excitation power [173].

In view of the great flexibility in both composition, structure and electronic band structures of 2D perovskites as well as the broad availability of layered materials, it is expected that there is still a large space to explore 2D perovskite-based heterostructures with new properties and advanced multifunctionalities.

6. Conclusion and outlooks

In this review, we have summarized the construction, characterizations, optical and optoelectronic properties as well as their potential applications of 2D perovskite-based heterostructures. Taking advantage of their layered nature, 2D perovskites can be mechanically exfoliated into thin flakes free of dangle bonds at surface from their respective bulk crystals and stack with other layered and non-layered materials to form heterostructures, which inherit the excellent optoelectronic properties of 2D perovskites and simultaneously introduce more new functionalities. Therefore, 2D perovskite-based heterostructures not only provide an exciting platform to explore rich photophysics, but also show promising potential applications in the field of optics and optoelectronics.

Despite substantial progress being made, studies on 2D perovskites with their heterostructures are still in preliminary stage and more investigations are required. First, it is still a challenge to obtain pure phase perovskites with a large layer number n, which is essential for constructing high-quality large n-number 2D perovskite heterostructures. Due to the similar thermodynamics of the crystalline process, it is difficult to synthesize very pure phase large n-number perovskites, which would hinder us to extract intrinsic physical properties of 2D perovskites and affect the performance of 2D perovskite optoelectronic devices. Similarly, heterostructures consisting of those hybrid-phase large n-number 2D perovskites would inherit those drawbacks mentioned above and also influence the interface of the heterostructure, both of which could impose more difficulties to study their intrinsic physical properties. Therefore, it is critical to first obtain high-quality pure phase 2D perovskites for constructing high-quality heterostructures.

Second, although a number of synthetic strategies have been developed to construct 2D perovskite-based heterostructures, there is still no universal method to rationally synthesize large-scale heterostructures with high crystalline quality in a controllable manner. The dry transfer method allows us to construct 2D perovskite heterostructure according to our design; nevertheless, this method cannot make large-scale heterostructures and the process is rather tedious and costly. In addition, the contamination can be introduced unintentionally at the interfaces during the transfer process, which would affect the quality of the heterostructures and subsequently deteriorate the performance of devices. Solution method cannot fabricate heterostructures with rather different compositions while the interfaces of heterostructures growing by vapor deposition method would be not sharp enough due to the ion diffusion during growing process. Controllably growing 2D perovskite heterostructures with a designed orientation are also critical

for optoelectronic devices due to the large electrical conductivity difference between in-plane and out-of-plane direction in 2D perovskites. Therefore, it is imperative to develop an efficient synthetic method to obtain large-area and high crystalline quality 2D perovskites heterostructures with controllable growth orientation.

Third, the rich physics in 2D perovskite-based heterostructures is still mostly unexplored. It is essential to systematically study the underlying physics of 2D perovskite-based heterostructures for potential optoelectronic applications. A large number of molecules can be selected as the organic cations for 2D perovskites, which provide an extra control knob to tune the properties of 2D perovskites although the electronic band structure of 2D perovskites is largely determined by the inorganic layer. For instance, how those organic cations affect the charge, energy transfer, and electron-phonon interaction in 2D perovskite-based heterostructures needs to be clarified so that the suitable organic cations could be selected to achieve optimized performance of optoelectronic devices. By replacing the organic cations with a conductive organic layer, the electrical conductivity along the out-of-plane direction might be improved, which would be beneficial to optoelectronic devices. In addition, the organic cations can introduce lattice distortion of the inorganic layer, leading to the formation of self-trapped excitons. Depending on the species of the organic cations, the degree of lattice distortion varies, which also can be used to tune the emission properties of 2D perovskite heterostructures. Furthermore, the chiral organic cations can be incorporated into 2D perovskites, endowing 2D perovskites with chirality. As a result, chiral 2D perovskites in heterostructures would work as a spin source and inject spin-polarized carriers into other constituent materials to tune spin- and valley-related properties, which would find important applications in spintronics and valleytronics. Lastly, by properly selecting the organic cations, 2D perovskites can also exhibit ferroelectricity and those 2D perovskite-based heterostructures would expect to find important applications in the polarization-sensitive photodetectors and tunable light emission devices. Nevertheless, studies on the detailed physical process in chiral 2D perovskite and ferroelectric 2D perovskite-based heterostructures remain elusive.

Lastly, there is still a large space to explore the potential optoelectronic applications based on 2D perovskite heterostructures in view of the availability of 2D perovskites and other layered materials. Stacking two or more different materials together to form heterostructures and multi-heterostructures can not only inherit the properties of constituent components, but also introduce extra newly designed functionalities according to our demands. For instance, a heterostructure integrating a chiral 2D perovskite with a monolayer WSe_2 could host interlayer excitons and the formed interlayer excitons with a long lifetime also exhibit valley polarization due to the spin-polarized carrier injection from chiral 2D perovskites. Thus, chiral 2D perovskites can be used to manipulate the valley polarization of monolayer TMDs for valleytronic devices. In addition, since both chiral 2D perovskites and monolayer TMDs can sense linearly- and circularly-polarized light, stacking them together would extend the photoresponse wavelength range of full-Stokes polarimeters in view of the different bandgap between chiral 2D perovskites and monolayer TMDs. Furthermore, stacking chiral 2D perovskites with achiral 2D perovskites would endow achiral 2D perovskites with circularly-polarized light emission due to the spin transfer process, which provides great flexibility to tune the emission wavelength range of circularly-polarized light emission source by integrating chiral 2D perovskites with other layered emission materials. Based on the same principle, we believe that more 2D perovskite-based heterostructures with novel functionalities will be constructed, taking advantage of the great flexibility in composition, structure, and properties of 2D perovskites.

Acknowledgments

D L acknowledges the support from National Key Research and Development Program of China (2018YFA0704403), NSFC (62074064) and Innovation Fund of WNLO.

Conflict of interest

The authors declare no conflict of interest.

ORCID iDs

Yingying Chen https://orcid.org/0000-0003-4519-5836
Dehui Li https://orcid.org/0000-0002-5945-220X

References

[1] Novoselov K S, Mishchenko A, Carvalho A and Castro Neto A H 2016 2D materials and van der Waals heterostructures *Science* **353** aac9439
[2] Chen Z Z, Guo Y W, Wertz E and Shi J 2019 Merits and challenges of ruddlesden-popper soft halide perovskites in electro-optics and optoelectronics *Adv. Mater.* **31** 1803514
[3] Chen S and Shi G Q 2017 Two-dimensional materials for halide perovskite-based optoelectronic devices *Adv. Mater.* **29** 1605448
[4] Zhou X, Hu X Z, Yu J, Liu S Y, Shu Z W, Zhang Q, Li H Q, Ma Y, Xu H and Zhai T Y 2018 2D layered material-based van der Waals heterostructures for optoelectronics *Adv. Funct. Mater.* **28** 1706587
[5] Shi E Z, Gao Y, Finkenauer B P, Akriti C A H and Dou L T 2018 Two-dimensional halide perovskite nanomaterials and heterostructures *Chem. Soc. Rev.* **47** 6046–72
[6] Wang H, Liu F C, Fu W, Fang Z Y, Zhou W and Liu Z 2014 Two-dimensional heterostructures: fabrication, characterization, and application *Nanoscale* **6** 12250–72
[7] Jin C H, Ma E Y, Karni O, Regan E C, Wang F and Heinz T F 2018 Ultrafast dynamics in van der Waals heterostructures *Nat. Nanotechnol.* **13** 994–1003
[8] Shree S, Paradisanos I, Marie X, Robert C and Urbaszek B 2021 Guide to optical spectroscopy of layered semiconductors *Nat. Rev. Phys.* **3** 39–54
[9] Fang C, Wang H Z and Li D H 2021 Recent progress in two-dimensional ruddlesden–popper perovskite based heterostructures *2D Mater.* **8** 022006
[10] Das S, Pandey D, Thomas J and Roy T 2019 The role of graphene and other 2D materials in solar photovoltaics *Adv. Mater.* **31** 1802722

[11] Grancini G and Nazeeruddin M K 2019 Dimensional tailoring of hybrid perovskites for photovoltaics *Nat. Rev. Mater.* **4** 4–22

[12] He T W *et al* 2020 Reduced-dimensional perovskite photovoltaics with homogeneous energy landscape *Nat. Commun.* **11** 1672

[13] Wang J Y, Verzhbitskiy I and Eda G 2018 Electroluminescent devices based on 2D semiconducting transition metal dichalcogenides *Adv. Mater.* **30** 1802687

[14] Ross J S *et al* 2017 Interlayer exciton optoelectronics in a 2D heterostructure p-n junction *Nano Lett.* **17** 638–43

[15] Mei F, Sun D W, Mei S J, Feng J H, Zhou Y M, Xu J X and Xiao X H 2019 Recent progress in perovskite-based photodetectors: the design of materials and structures *Adv. Phys.* X **4** 1592709

[16] Flöry N, Ma P, Salamin Y, Emboras A, Taniguchi T, Watanabe K, Leuthold J and Novotny L 2020 Waveguide-integrated van der Waals heterostructure photodetector at telecom wavelengths with high speed and high responsivity *Nat. Nanotechnol.* **15** 118–24

[17] Zhang L H, Zhang X and Lu G 2020 Band alignment in two-dimensional halide perovskite heterostructures: type I or type II? *J. Phys. Chem. Lett.* **11** 2910–6

[18] Xu Z Q, Mendelson N, Scott J A, Li C, Abidi I H, Liu H W, Luo Z T, Aharonovich I and Toth M 2020 Charge and energy transfer of quantum emitters in 2D heterostructures *2D Mater.* **7** 031001

[19] Bradac C, Xu Z Q and Aharonovich I 2021 Quantum energy and charge transfer at two-dimensional interfaces *Nano Lett.* **21** 1193–204

[20] Froehlicher G, Lorchat E and Berciaud S 2018 Charge versus energy transfer in atomically thin graphene-transition metal dichalcogenide van der Waals heterostructures *Phys. Rev.* X **8** 011007

[21] Liu X, Pei J J, Hu Z H, Zhao W J, Liu S, Amara M R, Watanabe K, Taniguchi T, Zhang H and Xiong Q H 2020 Manipulating charge and energy transfer between 2D atomic layers via heterostructure engineering *Nano Lett.* **20** 5359–66

[22] Rivera P, Yu H Y, Seyler K L, Wilson N P, Yao W and Xu X D 2018 Interlayer valley excitons in heterobilayers of transition metal dichalcogenides *Nat. Nanotechnol.* **13** 1004–15

[23] Jiang Y, Chen S L, Zheng W H, Zheng B Y and Pan A L 2021 Interlayer exciton formation, relaxation, and transport in TMD van der Waals heterostructures *Light Sci. Appl.* **10** 72

[24] Alferov Z I, Andreev V M, Garbuzov D Z, Zhilyaev Y V, Morozov E P, Portnoi E L and Trofim V G 1971 Investigation of the influence of the AlAs-GaAs heterostructure parameters on the laser threshold current and the realization of continuous emission at room temperature *Sov. Phys. Semicond.* **4** 1573–5

[25] Chang C *et al* 2021 Recent progress on two-dimensional materials *Acta Phys. Chim. Sin.* **37** 2108017

[26] Randviir E P, Brownson D A C and Banks C E 2014 A decade of graphene research: production, applications and outlook *Mater. Today* **17** 426–32

[27] Novoselov K S, Jiang D, Schedin F, Booth T J, Khotkevich V V, Morozov S V and Geim A K 2005 Two-dimensional atomic crystals *Proc. Natl Acad. Sci. USA* **102** 10451–3

[28] Manzeli S, Ovchinnikov D, Pasquier D, Yazyev O V and Kis A 2017 2D transition metal dichalcogenides *Nat. Rev. Mater.* **2** 17033

[29] Li L K, Yu Y J, Ye G J, Ge Q Q, Ou X D, Wu H, Feng D L, Chen X H and Zhang Y B 2014 Black phosphorus field-effect transistors *Nat. Nanotechnol.* **9** 372–7

[30] Novoselov K S, Geim A K, Morozov S V, Jiang D, Zhang Y, Dubonos S V, Grigorieva I V and Firsov A A 2004 Electric field effect in atomically thin carbon films *Science* **306** 666–9

[31] Mouri S, Miyauchi Y and Matsuda K 2013 Tunable photoluminescence of monolayer MoS_2 via chemical doping *Nano Lett.* **13** 5944–8

[32] Ju L *et al* 2014 Photoinduced doping in heterostructures of graphene and boron nitride *Nat. Nanotechnol.* **9** 348–52

[33] Li Z W *et al* 2020 Efficient strain modulation of 2D materials via polymer encapsulation *Nat. Commun.* **11** 1151

[34] Neumann C *et al* 2015 Raman spectroscopy as probe of nanometre-scale strain variations in graphene *Nat. Commun.* **6** 8429

[35] Bai Y S *et al* 2020 Excitons in strain-induced one-dimensional moiré potentials at transition metal dichalcogenide heterojunctions *Nat. Mater.* **19** 1068–73

[36] Edelberg D, Kumar H, Shenoy V, Ochoa H and Pasupathy A N 2020 Tunable strain soliton networks confine electrons in van der Waals materials *Nat. Phys.* **16** 1097–102

[37] Ross J S *et al* 2013 Electrical control of neutral and charged excitons in a monolayer semiconductor *Nat. Commun.* **4** 1474

[38] Baugher B W H, Churchill H O H, Yang Y F and Jarillo-Herrero P 2014 Optoelectronic devices based on electrically tunable p-n diodes in a monolayer dichalcogenide *Nat. Nanotechnol.* **9** 262–7

[39] Peimyoo N *et al* 2021 Electrical tuning of optically active interlayer excitons in bilayer MoS_2 *Nat. Nanotechnol.* **16** 888–93

[40] Ross J S *et al* 2014 Electrically tunable excitonic light-emitting diodes based on monolayer WSe_2 p-n junctions *Nat. Nanotechnol.* **9** 268–72

[41] Zhang Y J, Oka T, Suzuki R, Ye J T and Iwasa Y 2014 Electrically switchable chiral light-emitting transistor *Science* **344** 725–8

[42] Zhao C *et al* 2017 Enhanced valley splitting in monolayer WSe_2 due to magnetic exchange field *Nat. Nanotechnol.* **12** 757–62

[43] Aivazian G, Gong Z R, Jones A M, Chu R L, Yan J, Mandrus D G, Zhang C W, Cobden D, Yao W and Xu X 2015 Magnetic control of valley pseudospin in monolayer WSe_2 *Nat. Phys.* **11** 148–52

[44] Kim J, Hong X P, Jin C H, Shi S F, Chang C Y S, Chiu M H, Li L J and Wang F 2014 Ultrafast generation of pseudo-magnetic field for valley excitons in WSe_2 monolayers *Science* **346** 1205–8

[45] Wang H Z, Fang C, Luo H M and Li D H 2019 Recent progress of the optoelectronic properties of 2D Ruddlesden-Popper perovskites *J. Semicond.* **40** 041901

[46] Mao L L, Stoumpos C C and Kanatzidis M G 2019 Two-dimensional hybrid halide perovskites: principles and promises *J. Am. Chem. Soc.* **141** 1171–90

[47] Leng K, Fu W, Liu Y P, Chhowalla M and Loh K P 2020 From bulk to molecularly thin hybrid perovskites *Nat. Rev. Mater.* **5** 482–500

[48] Qi X, Zhang Y P, Ou Q D, Ha S T, Qiu C W, Zhang H, Cheng Y B, Xiong Q H and Bao Q L 2018 Photonics and optoelectronics of 2D metal-halide perovskites *Small* **14** 1800682

[49] Passarelli J V *et al* 2020 Tunable exciton binding energy in 2D hybrid layered perovskites through donor-acceptor interactions within the organic layer *Nat. Chem.* **12** 672–82

[50] Chen Y N, Sun Y, Peng J J, Tang J H, Zheng K B and Liang Z Q 2018 2D ruddlesden-popper perovskites for optoelectronics *Adv. Mater.* **30** 1703487

[51] Zhang C, Li Y, Ma C L and Zhang Q C 2022 Recent progress of organic–inorganic hybrid perovskites in RRAM, artificial synapse, and logic operation *Small Sci.* **2** 2100086

[52] Min H *et al* 2021 Perovskite solar cells with atomically coherent interlayers on SnO_2 electrodes *Nature* **598** 444–50

[53] Blancon J *et al* 2018 Scaling law for excitons in 2D perovskite quantum wells *Nat. Commun.* **9** 2254

[54] Era M, Maeda K and Tsutsui T 1998 Self-organization approach to organic/inorganic quantum-well based on metal halide-based layer perovskite *Thin Solid Films* **331** 285–90

[55] Gan Z X, Cheng Y C, Chen W J, Loh K P, Jia B H and Wen X M 2021 Photophysics of 2D organic–inorganic hybrid lead halide perovskites: progress, debates, and challenges *Adv. Sci.* **8** 2001843

[56] Gauthron K *et al* 2010 Optical spectroscopy of two-dimensional layered $(C_6H_5C_2H_4\text{-}NH_3)_2\text{-}PbI_4$ perovskite *Opt. Express* **18** 5912–9

[57] Ishihara T, Takahashi J and Goto T 1990 Optical properties due to electronic transitions in two-dimensional semiconductors $(C_nH_{2n+1}NH_3)PbI_4$ *Phys. Rev.* B **42** 11099–107

[58] Zhao X M, Liu T R and Loo Y L 2022 Advancing 2D perovskites for efficient and stable solar cells: challenges and opportunities *Adv. Mater.* **34** 2105849

[59] Gao Y *et al* 2019 Molecular engineering of organic-inorganic hybrid perovskites quantum wells *Nat. Chem.* **11** 1151–7

[60] Traore B *et al* 2018 Composite nature of layered hybrid perovskites: assessment on quantum and dielectric confinements and band alignment *ACS Nano* **12** 3321–32

[61] Cheng X H, Han Y and Cui B B 2022 Fabrication strategies and optoelectronic applications of perovskite heterostructures *Adv. Opt. Mater.* **10** 2102224

[62] Wang H Z, Ma J Q and Li D H 2021 Two-dimensional hybrid perovskite-based van der Waals heterostructures *J. Phys. Chem. Lett.* **12** 8178–87

[63] Aubrey M L, Saldivar Valdes A, Filip M R, Connor B A, Lindquist K P, Neaton J B and Karunadasa H I 2021 Directed assembly of layered perovskite heterostructures as single crystals *Nature* **597** 355–9

[64] Zhang J R, Song X F, Wang L and Huang W 2022 Ultrathin two-dimensional hybrid perovskites toward flexible electronics and optoelectronics *Natl Sci. Rev.* **9** nwab129

[65] Sirbu D, Balogun F H, Milot R L and Docampo P 2021 Layered perovskites in solar cells: structure, optoelectronic properties, and device design *Adv. Energy Mater.* **11** 2003877

[66] Saparov B and Mitzi D B 2016 Organic-inorganic perovskites: structural versatility for functional materials design *Chem. Rev.* **116** 4558–96

[67] Stoumpos C C, Cao D H, Clark D J, Young J, Rondinelli J M, Jang J I, Hupp J T and Kanatzidis M G 2016 Ruddlesden–popper hybrid lead iodide perovskite 2D homologous semiconductors *Chem. Mater.* **28** 2852–67

[68] Mao L L, Ke W J, Pedesseau L, Wu Y L, Katan C, Even J, Wasielewski M R, Stoumpos C C and Kanatzidis M G 2018 Hybrid Dion-Jacobson 2D lead iodide perovskites *J. Am. Chem. Soc.* **140** 3775–83

[69] Li X T *et al* 2019 Two-dimensional Dion-Jacobson hybrid lead iodide perovskites with aromatic diammonium cations *J. Am. Chem. Soc.* **141** 12880–90

[70] Guo W, Yang Z, Dang J L and Wang M Q 2021 Progress and perspective in Dion-Jacobson phase 2D layered perovskite optoelectronic applications *Nano Energy* **86** 106129

[71] Straus D B and Kagan C R 2018 Electrons, excitons, and phonons in two-dimensional hybrid perovskites: connecting structural, optical, and electronic properties *J. Phys. Chem. Lett.* **9** 1434–47

[72] Cao D H, Stoumpos C C, Farha O K, Hupp J T and Kanatzidis M G 2015 2D homologous perovskites as light-absorbing materials for solar cell applications *J. Am. Chem. Soc.* **137** 7843–50

[73] Sheng X, Li Y H, Xia M and Shi E Z 2022 Quasi-2D halide perovskite crystals and their optoelectronic applications *J. Mater. Chem.* A **10** 19169–83

[74] Kim H, Huynh K A, Kim S Y, Le Q V and Jang H W 2020 2D and quasi-2D halide perovskites: applications and progress *Phys. Status Solidi* **14** 1900435

[75] Yuan M J *et al* 2016 Perovskite energy funnels for efficient light-emitting diodes *Nat. Nanotechnol.* **11** 872–7

[76] Splendiani A, Sun L, Zhang Y B, Li T S, Kim J, Chim C Y, Galli G and Wang F 2010 Emerging photoluminescence in monolayer MoS_2 *Nano Lett.* **10** 1271–5

[77] Dou L T *et al* 2015 Atomically thin two-dimensional organic-inorganic hybrid perovskites *Science* **349** 1518–21

[78] Yu J C *et al* 2019 Broadband extrinsic self-trapped exciton emission in Sn-doped 2D lead-halide perovskites *Adv. Mater.* **31** 1806385

[79] Shen H Z, Li J Z, Wang H Z, Ma J Q, Wang J, Luo H M and Li D H 2019 Two-dimensional lead-free perovskite $(C_6H_5C_2H_4NH_3)_2CsSn_2I_7$ with high hole mobility *J. Phys. Chem. Lett.* **10** 7–12

[80] Blancon J *et al* 2017 Extremely efficient internal exciton dissociation through edge states in layered 2D perovskites *Science* **355** 1288–92

[81] Saouma F O, Stoumpos C C, Wong J, Kanatzidis M G and Jang J I 2017 Selective enhancement of optical nonlinearity in two-dimensional organic-inorganic lead iodide perovskites *Nat. Commun.* **8** 742

[82] Liu W W, Xing J, Zhao J X, Wen X L, Wang K, Lu P X and Xiong Q H 2017 Giant two-photon absorption and its saturation in 2D organic–inorganic perovskite *Adv. Opt. Mater.* **5** 1601045

[83] Wang J *et al* 2019 Giant nonlinear optical response in 2D perovskite heterostructures *Adv. Opt. Mater.* **7** 1900398

[84] Li W C, Ma J Q, Wang H Z, Fang C, Luo H M and Li D H 2020 Biexcitons in 2D $(iso\text{-}BA)_2PbI_4$ perovskite crystals *Nanophotonics* **9** 2001–6

[85] McCall K M, Stoumpos C C, Kostina S S, Kanatzidis M G and Wessels B W 2017 Strong electron–phonon coupling and self-trapped excitons in the defect halide perovskites $A_3M_2I_9$ (A = Cs, Rb; M = Bi, Sb) *Chem. Mater.* **29** 4129–45

[86] Li J Z, Wang H Z and Li D H 2020 Self-trapped excitons in two-dimensional perovskites *Front. Optoelectron.* **13** 225–34

[87] Wu X X, Trinh M T, Niesner D, Zhu H M, Norman Z, Owen J S, Yaffe O, Kudisch B J and Zhu X Y 2015 Trap states in lead iodide perovskites *J. Am. Chem. Soc.* **137** 2089–96

[88] Hu T *et al* 2016 Mechanism for broadband white-light emission from two-dimensional (110) hybrid perovskites *J. Phys. Chem. Lett.* **7** 2258–63

[89] Thirumal K *et al* 2017 Morphology-independent stable white-light emission from self-assembled two-dimensional perovskites driven by strong exciton–phonon coupling to the organic framework *Chem. Mater.* **29** 3947–53

[90] Yangui A *et al* 2015 Optical investigation of broadband white-light emission in self-assembled organic–inorganic perovskite $(C_6H_{11}NH_3)_2PbBr_4$ *J. Phys. Chem.* C **119** 23638–47

[91] DeCrescent R A, Du X H, Kennard R M, Venkatesan N R, Dahlman C J, Chabinyc M L and Schuller J A 2020 Even-parity self-trapped excitons lead to magnetic dipole

radiation in two-dimensional lead halide perovskites *ACS Nano* **14** 8958–68
[92] Li J Z, Wang J, Ma J Q, Shen H Z, Li L, Duan X F and Li D H 2019 Self-trapped state enabled filterless narrowband photodetections in 2D layered perovskite single crystals *Nat. Commun.* **10** 806
[93] Wang H Z, Li L, Ma J Q, Li J Z and Li D H 2021 2D perovskite narrowband photodetector arrays *J. Mater. Chem.* C **9** 11085–90
[94] Li J Z, Ma J Q, Cheng X, Liu Z Y, Chen Y Y and Li D H 2020 Anisotropy of excitons in two-dimensional perovskite crystals *ACS Nano* **14** 2156–61
[95] Li L, Jin L, Zhou Y X, Li J Z, Ma J Q, Wang S, Li W C and Li D H 2019 Filterless polarization-sensitive 2D perovskite narrowband photodetectors *Adv. Opt. Mater.* **7** 1900988
[96] Ma J Q, Fang C, Chen C, Jin L, Wang J Q, Wang S, Tang J and Li D H 2019 Chiral 2D perovskites with a high degree of circularly polarized photoluminescence *ACS Nano* **13** 3659–65
[97] Ma J Q, Fang C, Liang L H, Wang H Z and Li D H 2021 Full-stokes polarimeter based on chiral perovskites with chirality and large optical anisotropy *Small* **17** 2103855
[98] Shi E Z and Dou L T 2020 Halide perovskite epitaxial heterostructures *Acc. Mater. Res.* **1** 213–24
[99] Castellanos-Gomez A, Buscema M, Molenaar R, Singh V, Janssen L, Van Der Zant H S J and Steele G A 2014 Deterministic transfer of two-dimensional materials by all-dry viscoelastic stamping *2D Mater.* **1** 011002
[100] Pan D X, Fu Y P, Spitha N, Zhao Y Z, Roy C R, Morrow D J, Kohler D D, Wright J C and Jin S 2021 Deterministic fabrication of arbitrary vertical heterostructures of two-dimensional Ruddlesden-Popper halide perovskites *Nat. Nanotechnol.* **16** 159–65
[101] Akriti *et al* 2021 Layer-by-layer anionic diffusion in two-dimensional halide perovskite vertical heterostructures *Nat. Nanotechnol.* **16** 584–91
[102] Fang C, Wang H Z, Shen Z X, Shen H Z, Wang S, Ma J Q, Wang J, Luo H M and Li D H 2019 High-performance photodetectors based on lead-free 2D ruddlesden-popper perovskite/MoS_2 heterostructures *ACS Appl. Mater. Interfaces* **11** 8419–27
[103] Fu Y P, Zheng W H, Wang X X, Hautzinger M P, Pan D X, Dang L N, Wright J C, Pan A L and Jin S 2018 Multicolor heterostructures of two-dimensional layered halide perovskites that show interlayer energy transfer *J. Am. Chem. Soc.* **140** 15675–83
[104] Wang J, Li J Z, Lan S G, Fang C, Shen H Z, Xiong Q H and Li D H 2019 Controllable growth of centimeter-sized 2D perovskite heterostructures for highly narrow dual-band photodetectors *ACS Nano* **13** 5473–84
[105] Wang H L *et al* 2020 Extremely low dark current MoS_2 photodetector via 2D halide perovskite as the electron reservoir *Adv. Opt. Mater.* **8** 1901402
[106] Shi E Z, Yuan B, Shiring S B, Gao Y, Guo Y, Su C, Lai M, Yang P, Kong J and Savoie B M 2020 Two-dimensional halide perovskite lateral epitaxial heterostructures *Nature* **580** 614–20
[107] Ham A, Kim T S, Kang M, Cho H and Kang K 2021 Strategies for chemical vapor deposition of two-dimensional organic-inorganic halide perovskites *iScience* **24** 103486
[108] Wang J, Li J Z, Tan Q H, Li L, Zhang J B, Zang J F, Tan P H, Zhang J and Li D H 2017 Controllable synthesis of two-dimensional Ruddlesden–Popper-type perovskite heterostructures *J. Phys. Chem. Lett.* **8** 6211–9
[109] Hwang B and Lee J S 2019 2D perovskite-based self-aligned lateral heterostructure photodetectors utilizing vapor deposition *Adv. Opt. Mater.* **7** 1801356
[110] Mandal T N and Jana A 2020 Lateral epitaxial heterostructures of halide perovskites for diode application *Matter* **3** 617–9
[111] Hong X P, Kim J, Shi S F, Zhang Y, Jin C H, Sun Y H, Tongay S, Wu J Q, Zhang Y F and Wang F 2014 Ultrafast charge transfer in atomically thin MoS_2/WS_2 heterostructures *Nat. Nanotechnol.* **9** 682–6
[112] Jonas D M, Lang M J, Nagasawa Y, Joo T and Fleming G R 1996 Pump−probe polarization anisotropy study of femtosecond energy transfer within the photosynthetic reaction center of *Rhodobacter sphaeroides* R26 *J. Phys. Chem.* **100** 12660–73
[113] Yang T F *et al* 2019 Ultrahigh-performance optoelectronics demonstrated in ultrathin perovskite-based vertical semiconductor heterostructures *ACS Nano* **13** 7996–8003
[114] Yang A *et al* 2019 Giant enhancement of photoluminescence emission in WS_2-two-dimensional perovskite heterostructures *Nano Lett.* **19** 4852–60
[115] Chen Y Y, Liu Z Y, Li J Z, Cheng X, Ma J Q, Wang H Z and Li D H 2020 Robust interlayer coupling in two-dimensional perovskite/monolayer transition metal dichalcogenide heterostructures *ACS Nano* **14** 10258–64
[116] Yao W D, Yang D, Chen Y Y, Hu J C, Li J Z and Li D H 2022 Layer-number engineered momentum-indirect interlayer excitons with large spectral tunability *Nano Lett.* **22** 7230–7
[117] Chen Y Y, Ma J Q, Liu Z Y, Li J Z, Duan X P and Li D H 2020 Manipulation of valley pseudospin by selective spin injection in chiral two-dimensional perovskite/monolayer transition metal dichalcogenide heterostructures *ACS Nano* **14** 15154–60
[118] Zhang Q, Linardy E, Wang X Y and Eda G 2020 Excitonic energy transfer in heterostructures of quasi-2D perovskite and monolayer WS_2 *ACS Nano* **14** 11482–9
[119] Li D, Li D, Yang A Q, Zhang H, Lai X X and Liang C J 2021 Electronic and optical properties of van der Waals heterostructures based on two-dimensional perovskite $(PEA)_2PbI_4$ and black phosphorus *ACS Omega* **6** 20877–86
[120] Liu B, Long M Q, Cai M Q and Yang J L 2018 Two-dimensional van der Waals heterostructures constructed via perovskite $(C_4H_9NH_3)_2XBr_4$ and black phosphorus *J. Phys. Chem. Lett.* **9** 4822–7
[121] Zhan G X *et al* 2022 Stimulating and manipulating robust circularly polarized photoluminescence in achiral hybrid perovskites *Nano Lett.* **22** 3961–8
[122] Franken P A, Hill A E, Peters C W and Weinreich G 1961 Generation of optical harmonics *Phys. Rev. Lett.* **7** 118–9
[123] Zhou Y X, Huang Y Y, Xu X L, Fan Z Y, Khurgin J B and Xiong Q H 2020 Nonlinear optical properties of halide perovskites and their applications *Appl. Phys. Rev.* **7** 041313
[124] Li G X, Zhang S and Zentgraf T 2017 Nonlinear photonic metasurfaces *Nat. Rev. Mater.* **2** 17010
[125] Chen Z H, Zhang Q, Zhu M L, Chen H, Wang X Y, Xiao S, Loh K P, Eda G, Meng J Q and He J 2021 In-plane anisotropic nonlinear optical properties of two-dimensional organic–inorganic hybrid perovskite *J. Phys. Chem. Lett.* **12** 7010–8
[126] Han X, Zheng Y S, Chai S Q, Chen S H and Xu J L 2020 2D organic-inorganic hybrid perovskite materials for nonlinear optics *Nanophotonics* **9** 1787–810
[127] Abbas M S, Hussain S, Zhang J Q, Wang B X, Yang C, Wang Z, Wei Z X and Ahmad R 2020 Orientationally engineered 2D/3D perovskite for high efficiency solar cells *Sustain. Energy Fuels* **4** 324–30
[128] Wang Z, Lu Y L, Xu Z H, Hu J L, Chen Y J, Zhang C L, Wang Y S, Guo F and Mai Y 2021 An embedding 2D/3D heterostructure enables high-performance FA-alloyed

flexible perovskite solar cells with efficiency over 20% *Adv. Sci.* **8** 2101856
[129] Ge C Y, Xue Y Z B, Li L, Tang B and Hu H L 2020 Recent progress in 2D/3D multidimensional metal halide perovskites solar cells *Front. Mater.* **7** 601179
[130] Wang Z P, Lin Q Q, Chmiel F P, Sakai N, Herz L M and Snaith H J 2017 Efficient ambient-air-stable solar cells with 2D–3D heterostructured butylammonium-caesium-formamidinium lead halide perovskites *Nat. Energy* **2** 17135
[131] Lin J T, Chu T C, Chen D G, Huang Z X, Chen H C, Li C S, Wu C I, Chou P T, Chiu C W and Chen H M 2021 Vertical 2D/3D heterojunction of tin perovskites for highly efficient HTM-free perovskite solar cell *ACS Appl. Energy Mater.* **4** 2041–8
[132] Wang Q X *et al* 2020 Optoelectronic properties of a van der Waals WS_2 monolayer/2D perovskite vertical heterostructure *ACS Appl. Mater. Interfaces* **12** 45235–42
[133] Wang Q X and Wee A T S 2021 Upconversion photovoltaic effect of WS_2/2D perovskite heterostructures by two-photon absorption *ACS Nano* **15** 10437–43
[134] Bae S H, Kum H, Kong W, Kim Y, Choi C, Lee B, Lin P, Park Y and Kim J 2019 Integration of bulk materials with two-dimensional materials for physical coupling and applications *Nat. Mater.* **18** 550–60
[135] Liu Y, Guo J, Zhu E B, Liao L, Lee S J, Ding M N, Shakir I, Gambin V, Huang Y and Duan X F 2018 Approaching the schottky–mott limit in van der Waals metal–semiconductor junctions *Nature* **557** 696–700
[136] Yu W J, Liu Y, Zhou H L, Yin A X, Li Z, Huang Y and Duan X F 2013 Highly efficient gate-tunable photocurrent generation in vertical heterostructures of layered materials *Nat. Nanotechnol.* **8** 952–8
[137] Tan Z J *et al* 2016 Two-dimensional $(C_4H_9NH_3)_2PbBr_4$ perovskite crystals for high-performance photodetector *J. Am. Chem. Soc.* **138** 16612–5
[138] Cao Y *et al* 2022 Enhanced photodetector performance of black phosphorus by interfacing with chiral perovskite *Nano Res.* **15** 7492–7
[139] Feng F, Wang T, Qiao J, Min C J, Yuan X C and Somekh M 2021 Plasmonic and graphene-functionalized high-performance broadband quasi-two-dimensional perovskite hybrid photodetectors *ACS Appl. Mater. Interfaces* **13** 61496–505
[140] Zhang X Y, Liu X T, Li L N, Ji C M, Yao Y P and Luo J H 2021 Great amplification of circular polarization sensitivity via heterostructure engineering of a chiral two-dimensional hybrid perovskite crystal with a three-dimensional $MAPbI_3$ crystal *ACS Cent. Sci.* **7** 1261–8
[141] He Y H, Pan W T, Guo C J, Zhang H M, Wei H T and Yang B 2021 3D/2D perovskite single crystals heterojunction for suppressed ions migration in hard x-ray detection *Adv. Funct. Mater.* **31** 2104880
[142] Ahn J, Lee E, Tan J W, Yang W, Kim B and Moon J 2017 A new class of chiral semiconductors: chiral-organic-molecule-incorporating organic–inorganic hybrid perovskites *Mater. Horiz.* **4** 851–6
[143] Zhou H B, Lai H J, Sun X, Zhang N, Wang Y, Liu P Y, Zhou Y and Xie W G 2022 Van der Waals MoS_2/two-dimensional perovskite heterostructure for sensitive and ultrafast sub-band-gap photodetection *ACS Appl. Mater. Interfaces* **14** 3356–62
[144] Wang N N *et al* 2016 Perovskite light-emitting diodes based on solution-processed self-organized multiple quantum wells *Nat. Photon.* **10** 699–704
[145] Long G K *et al* 2018 Spin control in reduced-dimensional chiral perovskites *Nat. Photon.* **12** 528–33
[146] Zhao B D *et al* 2018 High-efficiency perovskite–polymer bulk heterostructure light-emitting diodes *Nat. Photon.* **12** 783–9
[147] Heo S *et al* 2019 Dimensionally engineered perovskite heterostructure for photovoltaic and optoelectronic applications *Adv. Energy Mater.* **9** 1902470
[148] Zhang J, Zhu X X, Wang M S and Hu B 2020 Establishing charge-transfer excitons in 2D perovskite heterostructures *Nat. Commun.* **11** 2618
[149] Xie C, Liu C K, Loi H L and Yan F 2020 Perovskite-based phototransistors and hybrid photodetectors *Adv. Funct. Mater.* **30** 1903907
[150] Shao Y C *et al* 2017 Stable graphene-two-dimensional multiphase perovskite heterostructure phototransistors with high gain *Nano Lett.* **17** 7330–8
[151] Fu Q D *et al* 2019 Ultrathin ruddlesden-popper perovskite heterojunction for sensitive photodetection *Small* **15** 1902890
[152] Leng K *et al* 2020 Electron tunneling at the molecularly thin 2D perovskite and graphene van der Waals interface *Nat. Commun.* **11** 5483
[153] Zhao L F, Tian H, Silver S H, Kahn A, Ren T L and Rand B P 2018 Ultrasensitive heterojunctions of graphene and 2D perovskites reveal spontaneous iodide loss *Joule* **2** 2133–44
[154] Jiang J Y, Zou X M, Lv Y W, Liu Y, Xu W T, Tao Q Y, Chai Y and Liao L 2020 Rational design of Al_2O_3/2D perovskite heterostructure dielectric for high performance MoS_2 phototransistors *Nat. Commun.* **11** 4266
[155] Schaibley J R, Yu H Y, Clark G, Rivera P, Ross J S, Seyler K L, Yao W and Xu X D 2016 Valleytronics in 2D materials *Nat. Rev. Mater.* **1** 16055
[156] Mak K F, He K L, Shan J and Heinz T F 2012 Control of valley polarization in monolayer MoS_2 by optical helicity *Nat. Nanotechnol.* **7** 494–8
[157] Cao T *et al* 2012 Valley-selective circular dichroism of monolayer molybdenum disulphide *Nat. Commun.* **3** 887
[158] Zeng H L, Dai J F, Yao W, Xiao D and Cui X D 2012 Valley polarization in MoS_2 monolayers by optical pumping *Nat. Nanotechnol.* **7** 490–3
[159] Kioseoglou G, Hanbicki A T, Currie M, Friedman A L, Gunlycke D and Jonker B T 2012 Valley polarization and intervalley scattering in monolayer MoS_2 *Appl. Phys. Lett.* **101** 221907
[160] Xiao D, Liu G B, Feng W X, Xu X D and Yao W 2012 Coupled spin and valley physics in monolayers of MoS_2 and other group-VI dichalcogenides *Phys. Rev. Lett.* **108** 196802
[161] Son J, Kim K H, Ahn Y H, Lee H W and Lee J 2019 Strain engineering of the berry curvature dipole and valley magnetization in monolayer MoS_2 *Phys. Rev. Lett.* **123** 036806
[162] Norden T, Zhao C, Zhang P Y, Sabirianov R, Petrou A and Zeng H 2019 Giant valley splitting in monolayer WS_2 by magnetic proximity effect *Nat. Commun.* **10** 4163
[163] Ye Y, Xiao J, Wang H L, Ye Z L, Zhu H Y, Zhao M, Wang Y, Zhao J H, Yin X B and Zhang X 2016 Electrical generation and control of the valley carriers in a monolayer transition metal dichalcogenide *Nat. Nanotechnol.* **11** 598–602
[164] Lu H P, Wang J Y, Xiao C X, Pan X, Chen X H, Brunecky R, Berry J J, Zhu K, Beard M C and Vardeny Z V 2019 Spin-dependent charge transport through 2D chiral hybrid lead-iodide perovskites *Sci. Adv.* **5** eaay0571
[165] Lu H P *et al* 2020 Highly distorted chiral two-dimensional tin iodide perovskites for spin polarized charge transport *J. Am. Chem. Soc.* **142** 13030–40
[166] Lagarde D, Bouet L, Marie X, Zhu C R, Liu B L, Amand T, Tan P H and Urbaszek B 2014 Carrier and polarization dynamics in monolayer MoS_2 *Phys. Rev. Lett.* **112** 047401

[167] Mai C, Barrette A, Yu Y F, Semenov Y G, Kim K W, Cao L Y and Gundogdu K 2014 Many-body effects in valleytronics: direct measurement of valley lifetimes in single-layer MoS_2 *Nano Lett.* **14** 202–6
[168] Rivera P *et al* 2015 Observation of long-lived interlayer excitons in monolayer $MoSe_2$–WSe_2 heterostructures *Nat. Commun.* **6** 6242
[169] Rivera P, Seyler K L, Yu H Y, Schaibley J R, Yan J Q, Mandrus D G, Yao W and Xu X D 2016 Valley-polarized exciton dynamics in a 2D semiconductor heterostructure *Science* **351** 688–91
[170] Nayak P K *et al* 2017 Probing evolution of twist-angle-dependent interlayer excitons in $MoSe_2$/WSe_2 van der Waals heterostructures *ACS Nano* **11** 4041–50
[171] Wei Q L, Wen X L, Hu J C, Chen Y Y, Liu Z Y, Lin T H and Li D H 2022 Site-controlled interlayer coupling in WSe_2/2D perovskite heterostructure *Sci. China Mater.* **65** 1337–44
[172] Tian H, Wang X F, Wu F, Yang Y and Ren T L 2018 High performance 2D perovskite/graphene optical synapses as artificial eyes *Proc. 2018 IEEE Int. Electron Devices Meeting* (San Francisco, CA: IEEE) pp 38.6.1–4
[173] Li Y T *et al* 2019 Light-enhanced ion migration in two-dimensional perovskite single crystals revealed in carbon nanotubes/two-dimensional perovskite heterostructure and its photomemory application *ACS Cent. Sci.* **5** 1857–65
[174] Ran C X, Xi J, Gao W Y, Yuan F, Lei T, Jiao B, Hou X and Wu Z W 2018 Bilateral interface engineering toward efficient 2D–3D bulk heterojunction tin halide lead-free perovskite solar cells *ACS Energy Lett.* **3** 713–21
[175] Gharibzadeh S *et al* 2019 Record open-circuit voltage wide-bandgap perovskite solar cells utilizing 2D/3D perovskite heterostructure *Adv. Energy Mater.* **9** 1803699
[176] La-Placa M G, Gil-Escrig L, Guo D Y, Palazon F, Savenije T J, Sessolo M and Bolink H J 2019 Vacuum-deposited 2D/3D perovskite heterojunctions *ACS Energy Lett.* **4** 2893–901
[177] Lin Y, Bai Y, Fang Y J, Chen Z L, Yang S, Zheng X P, Tang S, Liu Y, Zhao J J and Huang J S 2018 Enhanced thermal stability in perovskite solar cells by assembling 2D/3D stacking structures *J. Phys. Chem. Lett.* **9** 654–8
[178] Li P W, Zhang Y Q, Liang C, Xing G C, Liu X L, Li F Y, Liu X T, Hu X T, Shao G S and Song Y L 2018 Phase pure 2D perovskite for high-performance 2D–3D heterostructured perovskite solar cells *Adv. Mater.* **30** 1805323
[179] Zhang T K *et al* 2018 Stable and efficient 3D-2D perovskite-perovskite planar heterojunction solar cell without organic hole transport layer *Joule* **2** 2706–21
[180] Hu J L *et al* 2020 Spontaneously self-assembly of a 2D/3D heterostructure enhances the efficiency and stability in printed perovskite solar cells *Adv. Energy Mater.* **10** 2000173
[181] Grancini G *et al* 2017 One-year stable perovskite solar cells by 2D/3D interface engineering *Nat. Commun.* **8** 15684
[182] Ma C Y *et al* 2016 2D/3D perovskite hybrids as moisture-tolerant and efficient light absorbers for solar cells *Nanoscale* **8** 18309–14
[183] Hu Y H, Schlipf J, Wussler M, Petrus M L, Jaegermann W, Bein T, Müller-Buschbaum P and Docampo P 2016 Hybrid perovskite/perovskite heterojunction solar cells *ACS Nano* **10** 5999–6007
[184] Zhang X Y, Li L N, Ji C M, Liu X T, Li Q, Zhang K, Peng Y, Hong M C and Luo J H 2021 Rational design of high-quality 2D/3D perovskite heterostructure crystals for record-performance polarization-sensitive photodetection *Natl Sci. Rev.* **8** nwab044
[185] Lan Z J, Lau Y S, Wang Y W, Xiao Z, Ding L M, Luo D and Zhu F R 2020 Filter-free band-selective organic photodetectors *Adv. Opt. Mater.* **8** 2001388